Calcium dynamics of isolated Goldfish (*Carassius auratus*) retinal horizontal cells: Effects of oxygen-glucose deprivation

Benjamin Campbell

Thesis submitted to the
University of Ottawa
Faculty of Graduate and Postdoctoral Studies
in partial fulfillment of the requirements for the
MSc Degree of the
Ottawa-Carleton Institute of Biology

Department of Biology
Faculty of Science

26th of March, 2015 CE

Acknowledgements

First and foremost, I'd like to thank Michael Jonz for giving me the opportunity to play with horizontal cells for the past few years; providing guidance, support, and provoking curiosity (while keeping me focused on the big picture). You've grown my appreciation for science, and made my introduction to research all that it should be (and more!). I also thank the members of my committee, Jean-Marc Renaud, John Lewis, and Bill Willmore, for their insight throughout my masters, as well as Tuan Bui for agreeing to participate in my defence.

Secondly, I thank all Jonz Lab members past and present who've accompanied me. Especially, former grad students Peter "Beardo" Zachar for his ion channel wisdom (and loud music), as well as Sara "Cher" Abdallah, for her calcium imaging wisdom (and encouragement of silliness). Thanks to the current undergrads Freddy Nguyen and Sam Rahbar, and grad students Michael Country and Wen Pan for keeping the lab a fun and encouraging place. Also, thanks to the comparative physiology community of the Department of Biology for creating a great community where beer and science mix wonderfully. This thesis was funded in part by an NSERC PGSM award. Animal experiments were made possible by the folks at the Aquatics Facility, especially Bill Fletcher: so long and thanks for all the fish!

Finally I'd like to thank Mary "the rock" LaPierre for her many hugs and shared excitement for our next step together in the scientific world; as well as my family, especially my parents, for giving me endless food, support, and late night lab pickups.

Table of Contents:

List of Tables and Figures

...

...

List of Abbreviations

- μM = Micromolar (micromols quantity/ L solvent)
- [x] = the concentration of x
- $[x]_e$ = the extracellular concentration of x
- $[x]_i$ = the intracellular concentration of x
- x_e = extracellular x
- x_i = intracellular x
- AC = Amacrine cell
- AMPA = α-amino-3-hydroxy-5-methyl-4-isoxazolepropionic acid
- AMPA-R = AMPA receptor
- ADP = Adenosine diphosphate
- AMP = Adenosine monophosphate
- ATP = Adenosine triphosphate
- BC = Bipolar cell
- Ca^{2+} = Calcium ion
- $CaCl_2$ = Calcium chloride
- CCAC Canadian council on animal care
- Cd^{2+} = Cadmium ion
- $CdCl_2$ = Cadmium chloride
- Cl^- = Chloride ion
- CNS = Central nervous system
- Cs^+ = Cesium ion
- CsCl = Cesium chloride
- Cx = Connexin
- DMSO = Dimethyl sulphoxide
- ECS = Extra-cellular solution (various compositions See Table I)
- EGTA = Ethylene glycol-bis(2-aminoethylether)-N,N,N′,N′-tetraacetic acid
- ERG = Electroretinogram
- GABA = γ-Aminobutyric acid
- GAD = Glutamate decarboxylase
- GAT = GABA aminotransferase
- GC = Ganglion cell
- GCL = Ganglion cell Layer
- GJ = Gap junction
- GluR = glutamate receptor subunit
- h = hour
- H^+ = proton
- HC = Horizontal cell
- HCAT = Horizontal cell axon terminal
- HEPES = 2-[4-(2-hydroxyethyl)piperazin-1-yl]ethanesulfonic acid (a zwitterionic buffer)
- K^+ = Potassium ion
- KCl = Potassium chloride
- I_{Ca} = Calcium current
- I_{glu} = glutamate-elicited current
- iGluR = Ionotropic glutamate receptor

- INL = Inner nuclear layer
- IPC = Interplexiform cell
- IPL = Inner plexiform layer
- KA-R = Kainate receptor
- l = Litre
- LDH = Lactate dehydrogenase
- MC = Müller cell
- $MgCl_2$ = Magnesium chloride
- min = A minute
- mK_{ATP} = the mitochondrial ATP-sensitive K^+ channel
- mM = Millimolar
- Na^+ = Sodium ion
- Na^+/K^+ exchanger = the electrogenic membrane Na^+/K^+ exchanger
- NaCl = Sodium chloride
- Na_2HPO_4 = Sodium phosphate dibasic
- nm = Nanometres
- nM= nanomolar
- NMDA = N-methyl-D-aspartate
- NMDA-R = NMDA receptor
- O_2 = Molecular oxygen
- ONL = Outer nuclear layer
- OPL = Outer plexiform layer
- pH_i = intracellular pH
- PO_2 = Partial pressure of oxygen
- PR = Photoreceptor cell
- Px = Pannexin
- ROS = Reactive oxygen species
- RPE = Retinal pigment epithelium
- s = Seconds
- SOC = Store-operated channel
- VG (X) = a voltage gated channel permeating ion X
- V_m = membrane potential

Abstract

Studies on the survival of central nervous system of hypoxia-tolerant species under challenges of reduced energy availability have characterised adaptive mechanisms of brain at the cell and tissue level that lead to reduced excitability and protection. However, evidence of hypoxic suppression of retinal activity in these species has not been followed up with mechanistic studies. Microspectrofluorometric monitoring of intracellular free Ca^{2+} concentration ($[Ca^{2+}]_i$) is useful for identifying cellular mechanisms that may lead to adaptive strategies, as unregulated increases in $[Ca^{2+}]_i$ cause toxicity. Horizontal cells (HCs) are second order retinal neurons that receive tonic excitatory input from photoreceptors, and possess voltage-gated Ca^{2+} conductances and other channels that can facilitate toxic increases in $[Ca^{2+}]_i$ under conditions of reduced energy availability (modeled as oxygen-glucose deprivation, OGD). It was demonstrated that isolated HCs of the hypoxia-tolerant goldfish display spontaneous, transient $[Ca^{2+}]_i$ activity (SA) which decreased in amplitude and area under the curve following OGD or glucose removal (20 min) without recovery. SA was shown to be dependent on extracellular Ca^{2+} influx through voltage-gated Ca^{2+} channels, though mechanisms of SA generation and regulation has yet to be determined. Additionally, glutamate-elicited peak increases in $[Ca^{2+}]_i$ were reduced after 20 min of OGD. The removal of O_2 during OGD insult seemed to be protective as an increase in baseline $[Ca^{2+}]_i$ was seen during and following glucose removal under normoxic conditions. The mechanisms mediating these decreases in spontaneous and elicited $[Ca^{2+}]_i$ activity are currently unknown, though candidate pathways are discussed. This thesis contributes a hint towards how HCs may tolerate conditions of low energy availability, which may also inform investigations on their role *in situ* during these insults.

Résumé

Des études sur la survie des cerveaux des espèces qui sont tolérant à l'hypoxie sous défis de la disponibilité d'énergie réduite ont caractérisé les mécanismes d'adaptation au niveau des cellules et des tissus qui mènent à la réduction d'excitabilité et à la protection. Toutefois, la preuve de la suppression d'activité rétinienne causée par l'hypoxie chez ces espèces n'a pas été suivie d'études mécanistes. La mesure microspectrofluorométrique de la concentration de Ca^{2+} libre intracellulaire ($[Ca^{2+}]_i$) est utile pour identifier des mécanismes cellulaires qui peuvent mener à des stratégies d'adaptation, puisque des augmentations non-réglementée de $[Ca^{2+}]_i$ causent la toxicité. Les cellules horizontales (HCs) sont des neurones rétiniens de deuxième-ordre qui reçoivent l'entrée excitatrice tonique de photorécepteurs, et qui possèdent conductances de Ca^{2+} voltage-dépendants et d'autres canaux qui facilitent les augmentations toxiques de $[Ca^{2+}]_i$ dans des conditions de disponibilité réduite d'énergie (modélisé comme la deprivation d'oxygène-glucose, OGD). Il a été démontré que les HC isolés de poissons rouges, qui sont tolérant à l'hypoxie, possèdent de l'activité spontanée (SA) transitoire de $[Ca^{2+}]_i$ qui a diminué en amplitude et en aire sous la courbe suivant l'OGD ou l'élimination de glucose (20 min) sans récupération. SA a été démontré d'être dépendant sur l'afflux de Ca^{2+} extracellulaire par canaux Ca^{2+} voltage-dépendants, mais les mécanismes de production et de la réglementation de SA n'ont pas encore été déterminés. En outre, les augmentations maximales de $[Ca^{2+}]_i$ induites par le glutamate ont été réduits après 20 min d'OGD. L'élimination d'O_2 pendant l'OGD semblait avoir un effet protecteur puisqu'une augmentation des niveaux de base de $[Ca^{2+}]_i$ a été observée pendant et après l'élimination de glucose dans des conditions normoxiques. Les mécanismes qui médisent ces diminutions d'activité de $[Ca^{2+}]_i$ spontanée et provoquée sont actuellement inconnus, bien que des voies postulées sont discutées. Cette thèse contribue un indice envers

comment les HC peuvent tolérer des conditions de faible disponibilité d'énergie, qui peut également informer les enquêtes sur leur rôle in situ au cours de ces insultes.

1. Literature Review:

Hypoxia and ischemia are both conditions that may result in reduced energy availability which can limit the normal functioning of cells and tissues; encountered environmentally or as a consequence of both normal physiological function and disease states. Many vertebrates succumb to central nervous system (CNS) damage within minutes of these challenges, though several species, including the goldfish (*Carassius auratus*) have evolved adaptive mechanisms that allow them to survive for hours, days, or even longer. The purpose of this section is to review the physiological consequences of CNS hypoxia and ischemia, while identifying adaptive strategies employed by tolerant organisms. As an extension of the brain, the retina is similarly susceptible to reduced O_2 due to its high metabolic rate, and therefore is labile to hypoxic and ischemic stressors. Despite this, little is known about how retinal neurons from hypoxia-tolerant species are able to survive these insults. Goldfish horizontal cells (HCs) may provide a model of hypoxic and ischemic tolerance. The characterisation and function of retinal HCs will be discussed with a focus on their ionoregulatory and membrane characteristics as well as why these cells are an interesting model to examine responses to conditions of reduced energy availability.

1.1 Hypoxia and Ischemia Tolerance and Intolerance in Vertebrates.

1.1.1 Conditions of Reduced Energy Availability - Relevance to Vertebrates

Hypoxia and ischemia are distinct but often related challenges for cells, tissues, and whole organisms under different environmental, physiological, and pathophysiological states. Hypoxia can be defined environmentally as a decrease in the partial pressure of O_2 (PO_2) below ambient levels of 21% (Pamenter, 2014). Hypoxia can also be defined physiologically as the concentration of O_2 where aerobic metabolic function is limited (Renshaw & Nikinmaa, 2007),

as O_2 is required for oxidative phosphorylation and other O_2-dependent processes (Nilsson & Lutz, 1993; Fago & Jensen, 2015). Physiological hypoxia is produced by reduced O_2 delivery to tissues and/or increased O_2 consumption. For most vertebrates, O_2 is extracted from the environment by specially-designed structures such as lungs (mammals and other air breathers) or gills (water breathers such as fish), and delivered to cells and tissues by blood circulation. Therefore, physiological hypoxia can be generated by altered environmental availability, extraction efficiency, regulation of blood flow to tissues, and consumption at the cellular level.

The environmental availability of O_2 is far more variable for aquatic vertebrates such as amphibians and fish than for mammals (Bickler & Buck, 2007). The concentration of O_2 in aquatic habitats is reduced by increasing temperature (Nikinmaa, 2002), water stagnation (Walsh *et al.*, 2007), degradation of organic matter (Dorigatti *et al.*, 1997), as well as diurnal and seasonal changes like ice cover (Nilsson, 2001). Terrestrial vertebrates enjoy a much more constant supply of O_2, decreasing though with increasing altitude, and in contained habitats like burrows (Bickler & Buck, 1998; Galli & Richards, 2014).

At constant environmental levels, O_2 extraction is limited by the efficiency of gill and lung structures. Optimising these relies on decreasing the diffusion distance between the environment and the blood (Tzaneva *et al.*, 2014), and increasing the diffusion gradient by raising blood O_2 carrying capacity and employment of counter-current exchange systems (Waser & Heisler, 2005). After environmental extraction, O_2 delivery to cells requires efficient circulatory systems that are responsive to changes in O_2 demand.

Tissue O_2 demand varies with O_2 consumption, and is higher for more active tissues including the heart, CNS, and liver (Hochachka *et al.*, 1996). Within a certain range, vertebrates are able to regulate blood flow to increase O_2 delivery to demanding organs (Nilsson & Lutz,

2004), but this can still result in an insufficiency if demand exceeds supply, or under pathological states where blood flow is occluded (Lipton, 1999). Circumstances where blood flow to tissues is insufficient is defined as ischemia (Lipton, 1999; Osborne *et al.*, 2004). Tissue ischemia is often functionally related to tissue hypoxia in that a lack of blood flow reduces O_2 delivery, but is also accompanied by lowered delivery of energetic substrates such as glucose, and removal of metabolic by-products (Pamenter, 2014). Manifestations of acute pathological ischemia include heart attacks in cardiac tissue or stroke in the CNS (Contreras *et al.*, 2004). There are also deleterious effects of chronic ischemia, resulting in gradual development of diseases such as glaucoma (Osborne *et al.*, 2004). Both tissue hypoxia and ischemia are importantly linked by the low cellular availability of O_2. Although ischemia has been extensively studied in mammals, understanding mechanisms of ischemic survival are notably carried out in vertebrate models, such as the painted turtle and goldfish, as mechanisms of induced mammalian ischemic tolerance are similar to those found endogenously in these models of hypoxia tolerance (Galli & Richards, 2014; Pamenter, 2014).

1.1.2 Cellular Mechanisms of Hypoxic and Ischemic Damage

Before mechanisms of hypoxia and ischemia tolerance can be understood, the pathogenesis of intolerance must be discussed. Generally, both hypoxia and ischemia are problematic as they prevent normal cellular metabolic and functional processes rooted in restriction of sufficient energy production (Walsh *et al.*, 2007). If left unchecked, this can result in toxic self-reinforcing cascades: characterised by disruption of membrane potential, loss of ionic homeostasis, and $[Ca^{2+}]_i$ increases leading to necrotic or apoptotic cell death (Choi, 1992; Osborne *et al.*, 2004; Bickler & Buck, 2007). Under aerobic conditions, cellular adenosine

triphosphate (ATP) is efficiently generated by cytosolic glycolysis and subsequent oxidative phosphorylation of pyruvate or other catabolic metabolites in the mitochondria. Oxidative phosphorylation relies on using O_2 as the final electron acceptor in a redox transfer chain that generates a proton (H^+) gradient across the inner mitochondrial membrane. This transmembrane H^+ distribution allows for energy generation by H^+ current flow down its electrochemical gradient coupled to ATP production by ATP synthase. When O_2 is limiting, oxidative metabolism is suppressed (or is arrested in the absence of O_2), and anaerobic fermentation pathways become important in maintaining ATP supply. Vertebrate fermentation generates ATP from substrate-level phosphorylation in the cytoplasm, and the use the action of lactate dehydrogenase (LDH) to regenerate oxidised nicotinamide adenine dinucleotide (NAD^+), required for continued glycolytic flux, producing lactate in the process. Anaerobic ATP generation produces less than 1/10th that of aerobic conditions (Galli & Richards, 2014); therefore eventually ATP supply becomes uncoupled with ATP demand (Hochachka, 1986). This is a great concern for very metabolically-active cells including myocytes (Stensløkken *et al.*, 2014), hepatocytes (Buck & Hochachka, 1993; Staples & Buck, 2009), and especially neurons (Bickler, 1992, 2004). In these cells, the activity and maintenance of excitable membranes are important for cell function and survival.

Neurons establish a transmembrane voltage, primarily by the distribution of sodium (Na^+), potassium (K^+), calcium (Ca^{2+}), and chloride ions (Cl^-) ions. The separation of these ions across the membrane is driven by the activity of energy-dependent ion pumps and electrogenic exchangers. These gradients can become dissipated in time through active processes including ion exchange and signalling-related permeability changes, as well as passively via transmembrane leak of ions down their electrochemical gradient. In general, intracellular [Na^+]

and [Ca^{2+}], but not [K^{+}] levels are lower than extracellular levels. In order to maintain membrane polarity and excitability, ion gradients need to be continuously regenerated, requiring access to sufficient ATP. When O_2 levels decline past the point where oxidative ATP generation can match demand, transmembrane ion gradients collapse (Hochachka, 1986; Walsh *et al.*, 2007). K^{+} efflux and subsequent extracellular accumulation, as well as Na^{+} influx, depolarise the cell to threshold levels where voltage-gated ion channels open, including voltage-gated Ca^{2+} ($VGCa^{2+}$) channels, allowing further membrane depolarisation and increasing $[Ca^{2+}]_i$ (Hochachka, 1986; Boutilier, 2001). Unregulated increases in $[Ca^{2+}]_i$ can activate Ca^{2+}-dependent proteases and phospholipases; this may accelerate the loss of membrane integrity and ion homeostasis, ultimately leading to cell death (Choi, 1992; Boutilier, 2001).

Importantly for excitatory neurons, loss of ionic homeostasis causes reversal of Na^{+}-dependent glutamate uptake transporters (Bickler & Buck, 1998; Osborne *et al.*, 2004). Increased synaptic [glutamate] can activate post-synaptic ionotropic glutamate receptors (iGluR), causing harmful levels of Na^{+} and Ca^{2+} influx in neighboring cells, termed "excitotoxicity" (Choi, 1992; Bickler & Buck, 1998; Walsh *et al.*, 2007). There are several species of iGluRs known to mediate excitatory synaptic transmission in the vertebrate CNS including N-methyl-D-aspartate receptors (NMDA-Rs), α-Amino-3-hydroxy-5-methyl-4-isoxazolepropionic acid receptors (AMPA-Rs), and kainate receptors (KA-Rs). NMDA-Rs are often implicated as major contributors to excitotoxicity due to their relatively higher conductance of Ca^{2+} into the cell (Norris *et al.*, 2006). AMPA-Rs are also gaining respect as important mediators of Ca^{2+} influx under ischemic conditions (Kwak & Weiss, 2006). AMPA-Rs are composed of four subunits arranged as homo- or heteromeric structures of GluR1,2,3, and 4 subunits. AMPA-Rs lacking a GluR2 subunit show high Ca^{2+} permeability (Huang & Liang, 2005). iGluRs can also exacerbate

other influxes of Ca^{2+}: through $VGCa^{2+}$ channels, Ca^{2+}-induced Ca^{2+} release (CICR), Ca^{2+} release from the mitochondria (Norris *et al.*, 2006), and through hemichannel opening (Weilinger *et al.*, 2012). Hemichannels in vertebrates are either connexin (Cx) or pannexin (Px) type (Scemes *et al.*, 2009). Cx also commonly form gap junctions (GJ) between cells (allowing for electrical and cytosolic communication). Hemichannel conductance is generally large (200 and 500 pS) and non-selective (Scemes *et al.*, 2009), passing molecules and ions under 1 kDa (Contreras *et al.*, 2004; MacVicar & Thompson, 2010). Cx hemichannels open usually under conditions of low divalent ion concentration and supra-physiological depolarisations, whereas Px hemichannels open at physiological [Ca^{2+}] and membrane potentials (Scemes *et al.*, 2009). Ischemia modeled as oxygen-glucose deprivation (OGD) was shown to open neuronal hemichannels, contributing to ionic deregulation (Thompson *et al.*, 2006). Px hemichannels can also be activated by NMDA-R stimulation through an SRC family kinase dependent pathway, causing damage and anoxic depolarisation (Weilinger *et al.*, 2012). Interestingly, genetic ablation of Px expression was protective in ischemic retinal damage (Dvoriantchikova *et al.*, 2012).

Ischemia, though it involves components of hypoxia, also lowers the delivery of energetic substrates to tissues, and slows clearance of metabolic waste (Osborne *et al.*, 2004). Under conditions where anaerobic metabolism must support normal cell function, un-interrupted glycolytic substrate delivery is required to slow the rate of ATP decline (Bickler & Buck, 1998). In addition, increased reliance on fermentation pathways results in increased production of lactate and H^+ causing metabolic acidosis if allowed to build up in tissue (Shoubridge & Hochachka, 1980; Bickler & Buck, 2007). Hypoxic and ischemic acidosis has been linked to

amplification of neuronal damage, possibly through disrupted Ca^{2+} homeostasis, although mild acidosis has been implicated in neuroprotection (Osborne *et al.*, 2004).

Beyond issues of reduced ATP production, the signalling and destructive roles of reactive oxygen species (ROS) must be mentioned. ROS are produced by mitochondria during normal oxidative function. A fraction of O_2 is converted to the superoxide anion (O_2^-) at complex I and III of the electron transport chain (Galli & Richards, 2014). ROS can act as a signalling molecule, although excessive ROS production damages cells by lipid peroxidation, DNA damage, and activation of apoptotic death (Galli & Richards, 2014). Although ROS production relies on the presence of O_2, production can still occur during ischemia or hypoxia as long as residual O_2 is present (Galli & Richards, 2014). During oxidative function, cells are able to regulate ROS over-production using scavenging enzymes and antioxidants. During ischemia and hypoxia, the ROS buffering capacity of the cell is limited. Most damaging is ROS generation during ischemic reperfusion or re-oxygenation (Osborne *et al.*, 2004; Galli & Richards, 2014). There are many pathways that generate free radicals during re-oxygenation, linked to increases in $[Ca^{2+}]_i$, and oxidation of previously reduced compounds that accumulate during hypoxia (Osborne *et al.*, 2004). ROS generated during reperfusion can overwhelm endogenous defenses and becomes toxic, contributing to hypoxic and ischemic damage even after the initial insult (Lipton, 1999; Galli & Richards, 2014).

All of the mechanisms of hypoxic and ischemic damage mentioned in the above sections can lead to disruption at the level of the cell, but the interplay between these processes is complex, and made even more so when considering that hypoxia and ischemia occur at the tissue and organismal level. Within a tissue, some cells can be more sensitive to insults than others. For example neurons that receive glutamatergic input are more likely to be labile to excitotoxic

insults (Ankarcrona *et al.*, 1995). In addition, the interaction between cells becomes important considering that areas of apoptotic and necrotic cell death can expand even after the initial insult. Cerebral and retinal ischemia are described as a core of damage that occurs immediately as a result of the insult, surrounded by a penumbra that can be recruited into the core, with penumbral cells dying a delayed death (Lipton, 1999; Contreras *et al.*, 2004). The rate and mechanism of delayed cell death in ischemia are varied and are a product of the degree and duration of the insult (Lipton, 1999). Due to the great complexity in modelling hypoxia and ischemia holistically at the tissue or organ level, understanding the base mechanisms of damage and tolerance are often carried out in reduced systems like tissue slices and neuronal cultures (Lipton, 1999), and using lower complexity insults, for example hypoxia or oxygen-glucose deprivation as ischemic mimics (Weilinger *et al.*, 2012; Pamenter *et al.*, 2012).

1.1.3 The Retina as a CNS model for Hypoxic and Ischemic Insults

The retina offers an interesting model with which to investigate hypoxic and ischemic damage and tolerance. Although it is known as the primary light sensory organ in vertebrates, it is also composed of CNS neurons, being embryologically a projection of the forebrain (Kato *et al.*, 1991). Experimentally, the retina is useful because it is a visibly laminar structure, and the vast majority of the cell types are morphologically and biochemically distinct (Kato *et al.*, 1991). Being an externalised part of the CNS, its manipulation and monitoring can be achieved with less invasiveness and with greater ease. The retina can also be removed and kept functional for hours in isolation as an intact slice of the CNS (Rowe, 1987; Kato *et al.*, 1991).

The development and consequences of acute retinal damage are similar to those in other areas of the CNS (Osborne *et al.*, 2004; Schmidt *et al.*, 2008). Glutamate is the main excitatory

neurotransmitter of the retina, released constantly from photoreceptors in the dark. Many neurons in the retina express glutamate receptors and transporters (Ishikawa, 2013), and as such a finely tuned system of glutamate release and uptake from synapses is necessary (Ishikawa, 2013). Excessive glutamate release has been suggested to be the main cause of initial damage in acute retinal ischemia (Hankins & Ikeda, 1993; Osborne *et al.*, 2004).

The degree of damage of retinal hypoxia or ischemia can be measured histologically or by looking at the electrical waveform of the ERG (composed of 3 distinct electrical waves after stimulation with a flash of light). Altered ERG waves indicate malfunction, and a lack of recovery after re-perfusion indicates permanent damage (Osborne *et al.*, 2004). Retinal, like brain ischemia is a complex series of harmful events, but preventing glutamate toxicity, maintaining ion homeostasis, reducing free radical generation, and preventing large increases in $[Ca^{2+}]_i$ are thought to be important preventative strategies (Osborne *et al.*, 2004; Schmidt *et al.*, 2008; Szabadfi *et al.*, 2010).

1.1.4 General Mechanisms of Hypoxic and Ischemic Tolerance

As discussed, hypoxic and ischemic damage can have diverse aetiologies and physiological consequences, but are linked by the proximal issue of O_2 lack (Walsh *et al.*, 2007; Pamenter *et al.*, 2012). Well-studied hypoxia-tolerant species such as the painted turtle (*Chrysemys picta*), the Crucian carp (*Carassius carassius*), and its congeneric cousin the goldfish (*Carassius auratus*) (Lutz & Nilsson, 1997; Mandic *et al.*, 2008) have evolved adaptive mechanisms to combat the detrimental effects of low O_2 and reduced energy availability (Bickler & Buck, 1998). Some tolerant organisms employ simple behavioural adaptations to avoid or reduce the extent of hypoxia sustained. Behavioural adaptations of aquatic species include

avoidance of hypoxic water (Robinson *et al.*, 2013) as seen in goldfish (Ogilvie, 1982; Crawshaw *et al.*, 1989) and the use of surface respiration (Kramer, 1987). Physiological responses to hypoxia include increased ventilation (Kramer, 1987) and modification of gill structures (Tzaneva *et al.*, 2014) to maximise O_2 extraction. Still, if O_2 supply is limiting, other adaptive mechanisms of hypoxic survival must be employed.

Hochachka identified that tolerance and intolerance importantly lies in how cells and organisms balance energy production and energy demand (Hochachka, 1986; Hochachka *et al.*, 1996). Broadly, mammalian and endothermic vertebrates are thought to be less tolerant than their ectothermic relatives: amphibians and fish (Bickler & Buck, 2007) There are of course many exceptions to this generalisation. Trout are intolerant of hypoxia (Nilsson *et al.*, 1993), and zebrafish are only tolerant during early development (Padilla & Roth, 2001). In addition, hibernating mammals, like the arctic ground squirrel (Boutilier, 2001), and burrowers, like the naked mole rat (Pamenter, 2014) are more tolerant. Ischemia and hypoxia are damaging because they restrict normal ATP supply. So what separates these species across the tolerance spectrum may be rooted in the strategies of metabolic regulation employed.

One strategy of metabolic regulation is to try to sustain normoxic function by up-regulating glycolytic pathways. While this can increase ATP yield, this strategy is not sustainable because anaerobic fermentation is inefficient and produces toxic waste products (Bickler & Buck, 1998). Cells of organisms that rely solely on up-regulated glycolysis, eventually will lose energetic balance (Lutz & Nilsson, 1997). Another strategy employed is to reduce energy demand, while simultaneously matching energy production to a new, lower steady state level (Hochachka *et al.*, 1996; Lutz & Nilsson, 1997; Staples & Buck, 2009). The former strategy is characteristic of extremely intolerant organisms such as rats and humans who survive

for only a few minutes without permanent brain damage, while the latter represents the strategy taken by very tolerant organisms like painted turtle and goldfish who can withstand weeks without O_2 under the right conditions (Bickler & Buck, 1998; Bickler, 2004).

1.1.5 Resiliency of Hypoxia-tolerant Brains

Brain health under hypoxic and ischemic conditions can be monitored by gross electrical recordings (electroencephalograms, EEGs) and changes in intra/extracellular ion concentrations. In intolerant brains, including those of mammals, the rapid fall in brain ATP following an insult reduces the activity of the ATP-dependent Na^+/K^+ATPase within minutes, causing an extracellular increase in K^+ , intracellular increase in Na^+, and subsequent depolarisation (Bickler & Buck, 1998). On the other hand, brain ATP and extracellular K^+ levels of painted turtle (Lutz & Nilsson, 1997) and crucian carp (Nilsson *et al.*, 1993) remain constant even after hours of anoxia. Part of this maintenance of ATP levels comes from an up-regulation of glycolysis. Hypoxia-tolerant species have large glycogen stores (Lutz & Nilsson, 1997) and are able to manage lactate resulting from fermentation pathways (Nilsson, 2001; Bickler & Buck, 2007). Goldfish for example, convert excess lactate into ethanol that is excreted easily across the gills (Shoubridge & Hochachka, 1980). The *Carassius* brain is more dependent on glycolysis than that of the painted turtle, and inhibition of glycolysis during anoxia results in an increase in extracellular K^+, coinciding with a decrease in cellular ATP (a change not seen during normoxia, or in the painted turtle under long-term anoxia) (Johansson & Nilsson, 1995). This suggests that ATP demand is not suppressed to the extent that it is in the turtle. This difference in reliance on anaerobic ATP generation is likely a reflection of the degree to which metabolism is suppressed in these species (Lutz & Nilsson, 1997). *Carassius* reduces locomotory activity by over 50%

during anoxia, but still maintains swimming and can respond to stimuli (although visual and auditory systems are suppressed (Fay & Ream, 1992; Johansson *et al.*, 1997), whereas the painted turtle becomes comatose and unresponsive (Lutz *et al.*, 1996).

Both painted turtle and *Carassius* undergo a significant anoxic depression in whole organism and brain metabolic rate (over 40%) (Lutz *et al.*, 1996). The processes that mediate this decrease in metabolism may be due to decreased protein synthesis or changes in membrane permeability amongst other strategies (Hochachka, 1986; Bickler & Buck, 2007).

1.1.6 Cellular Mechanisms of CNS Tolerance

Decreasing membrane permeability is expected to be an important mechanism mediating metabolic depression. In the brain, up to 80% of ATP consumption is linked to maintaining ionic homeostasis through ion pumps (Bickler & Buck, 1998); therefore, decreasing membrane permeability would reduce ion translocation and the amount of ATP used by pumps. Decreased membrane permeability is facilitated either by reducing membrane leakiness or minimising permeability during active membrane processes, termed "ion channel arrest" (Hochachka, 1986). Channel arrest could be effected by changes in ion channel density, conductance characteristics, or channel isoforms expressed (Bickler & Buck, 1998). Anoxic suppression of the Na^+/K^+ATPase is seen in painted turtle and goldfish, but this also requires a coordinated reduction in membrane permeability to maintain ion gradients (Staples & Buck, 2009). In addition to brain Na^+ and K^+ gradients, levels of neuronal $[Ca^{2+}]_i$ are stable throughout anoxia (unlike in rat where levels rapidly increase to over 1 mM) (Bickler & Buck, 1998). Membrane permeability can be down-regulated in response to hypoxic challenge, for example Ca^{2+} influx in anoxic painted turtle brain occurs by inhibition of glycolysis, but only during the first few

minutes of anoxia. After long-term anoxia, there is no effect of glycolysis inhibition (Bickler, 1992), indicating that there may be arrest of Ca^{2+} channels, or other processes which can potentiate Ca^{2+} entry.

Most evidence for ion channel arrest comes from studies of iGluRs in the painted turtle brain, though there is evidence for arrest of other channel type. For example, voltage-gated Na^{+} ($VGNa^{+}$) channels decrease in density by 42% during anoxia in painted turtle brain (Pérez-Pinzón *et al.*, 1992). Both NMDA-R and AMPA-R activities are suppressed in the anoxic turtle brain, and this inhibition is required for neuronal survival (Bickler *et al.*, 2000). NMDA-R currents are suppressed by a 62% decrease in open probability within 15 min of anoxia (Buck & Bickler, 1998). Hypoxia was shown to suppress NMDA-R activity (both open probability and Ca^{2+} influx) by 50-60% within 1-8 min, via the activation of phosphatase 1/2a (Bickler *et al.*, 2000). These authors additionally showed that prolonged anoxia (hours) saw a modest increase in $[Ca^{2+}]_i$ that also suppressed NMDA-R activity via calmodulin. Calmodulin was shown to bind to dephosphorylated NR1 NMDA subunits causing a dissociation of the subunit from the cytoskeleton (Shin *et al.*, 2005). Upstream activation of mitochondrial K_{ATP} (mK_{ATP}) channels is required to cause the modest increase in $[Ca^{2+}]_i$ via uncoupling of mitochondria, and diminished Ca^{2+} uptake by the mitochondrial Ca^{2+} uniporter (Pamenter *et al.*, 2008*b*; Pamenter, 2014). Interestingly, a similar mK_{ATP}-related mechanism has been found in mammalian brain during ischemic preconditioning, where ischemia or anoxia of short duration primes neurons to survive otherwise toxic long ischemic bouts (Pamenter *et al.*, 2008*b*). Like NMDA-Rs, AMPA-R peak currents also decreased by 59% after 20 min of anoxia (Pamenter *et al.*, 2008*a*) acting again via mK_{ATP} channels (Zivkovic & Buck, 2010). It was assumed that ion channel arrest was a protective strategy adopted more by painted turtles since they are known to suppress their brain

activity to a greater extent than fish (Lushchak *et al.*, 2001; Stensløkken *et al.*, 2008*a*). Recently, hypoxia-induced ion channel arrest of NMDA-Rs has been confirmed in the goldfish brain, showing an 40-50% reduction in activity (Wilkie *et al.*, 2008). These authors also demonstrated a brain-specific reduction in goldfish Na^+/K^+ATPase activity under chronic hypoxia (Wilkie *et al.*, 2008), although a mechanism for down-regulation was not elucidated.

γ-Aminobutyric acid (GABA) is the main inhibitory neurotransmitter in the vertebrate brain and is thought to play an important role in brain metabolic depression in hypoxia-tolerant species (Nilsson & Lutz, 1993). It increases dramatically in the anoxic painted turtle brain, and less dramatically, but still importantly in anoxic *Carassius* brain (Nilsson & Lutz, 2004). GABA acts as an inhibitory neurotransmitter by lowering the excitability of neurons, binding to $GABA_A$ receptors (which allow Cl^- influx), and $GABA_B$ receptors (which allow for K^+ efflux). Thus GABA release under conditions of reduced energy availability can be protective (Buck *et al.*, 2012). GABA is synthesised from glutamate in an O_2-independent manner by glutamate decarboxylase (GAD), but GABA breakdown by GABA aminotransferase (GAT) requires the presence of O_2, allowing anaerobic accumulation of GABA (Nilsson & Lutz, 1993). Reduced GABA uptake has also been implicated in brain activity suppression in *Carassius* (Ellefsen *et al.*, 2008), and it likely to play a complimentary role to ion channel arrest in these species (Buck *et al.*, 2012)

Beyond metabolic arrest mechanisms, goldfish and painted turtles are also equipped to handle reperfusion damage from ROS by constitutively high levels of antioxidant defences (Willmore and Storey, 1997; Bickler & Buck, 2007). In the goldfish, antioxidant enzymes (e.g. glutathione peroxidase, catalase) undergo a sustained increase in anoxia, slowing brain lipid peroxidation during re-oxygenation (Lushchak *et al.*, 2001). Whereas in mammals, endogenous

antioxidants are overcome by free radical generation early during reperfusion (Lipton, 1999; Lushchak *et al.*, 2001).

Determining cellular mechanisms of hypoxic and ischemic resilience in hypoxia-tolerant organisms has focussed in large part on the brain, heart, and liver. Though, like the brain, teleost retinas have high metabolic rates, requiring abundant O_2 (Waser & Heisler, 2005). The retina is an often used model of CNS circuitry (as described below), and the *Carassius* genus is an often used model of hypoxia tolerance. Given this, it is surprising that there is very little information on hypoxic function of fish vision (Robinson *et al.*, 2013), and virtually none on retinal tolerance or the cellular responses of retinal cells to hypoxia or ischemia (Kato *et al.*, 1997*a*). What is known is that the fish retina is hypoxia-sensitive, and like the brain (in tolerant species at least), responds to conditions of low O_2 by reducing electrical activity and excitability (Stensløkken *et al.*, 2008*a*). The *Carassius* retina and optic tectum responds to hypoxia by a reduction (up to 90%) in light-evoked electrical activity that is fully reversible upon re-oxygenation (Johansson *et al.*, 1997). This reduction in responsiveness suggests that the activity of ion channels might be down-regulated (Nikinmaa, 2002), or may be mediated by a more global depression (e.g GABA-ergic signalling) (Johansson *et al.*, 1997). However, it is not currently known how retinal neurons of hypoxia-tolerant fish resist hypoxic or ischemic challenges. As will be elaborated in the next section, HCs of the goldfish retina may be a good starting point to investigate cellular responses to conditions of reduced energy availability in the retina of a hypoxia-tolerant organism.

1.2 Horizontal cells of the goldfish retina

1.2.1 The Teleost Retina - Conserved Model of CNS Circuitry

The teleost retina has been long used as a convenient model for studying central nervous system circuitry. Reasons for this include the retina's conserved anatomy and function across vertebrates, its well characterised cell types and cell to cell interaction, and is experimental ease of use as it is embryologically an externalisation of the forebrain, but is more accessible and amenable to experimental manipulation (reviewed in Kato, 1991).

Like in most vertebrates, the fish eye is bordered by the sclera, a protective outer layer that lies external to the choroid layer (which provides vascular support to the retina). In teleosts, blood supply occurs via a highly efficient rete mirabile counter-current exchange structure in the choroid which can provide high PO_2 levels for the metabolically-demanding retina (Hitchcock & Easter, 1986; Waser & Heisler, 2005). In order to form an image, light is focused by the cornea (a transparent section of the sclera), passes through the aqueous body, and is focused again by the lens, projecting the image through the vitreous body onto the retina (which sits internal to the choroid).

The retina is a light-sensitive structure that receives light input (photons), transforms this into electrical signals, and then processes the information before it outputs to the brain via the optic nerve (Kolb *et al.*, 2001; Thoreson & Mangel, 2012). Important processing by retinal neurons includes providing colour opponency (Twig *et al.*, 2003) as well as contrast discrimination (Thoreson & Mangel, 2012). Retinal structure, cell types, and general function are similar between vertebrates (Kolb *et al.*, 2001; Lenkowski & Raymond, 2014), but will be described here for teleosts, and specifically the goldfish which has a long history of use as a retinal model. Lasting descriptions of goldfish retinal cell types and connections have been

established, importantly linking retinal morphology and anatomy to physiological function (Stell, 1967; Parthe, 1972; Stell & Lightfoot, 1975).

1.2.2. Laminar and Functional Organisation of Retinal Cell Types

The retina is a multilayered layered laminar structure of CNS neurons and glia (see Fig. 1 for schematic diagram). Rod or cone photoreceptor (PRs) somas reside in the outer nuclear layer (ONL), while their light-sensitive outer segments protrude into the photoreceptor layer (PRL). Goldfish have one type of rod, and four types of cone, subdivided based on their morphology, pigment content (absorbance maxima at 455, 530, or 625 nm which is similar to those of humans), and response to light spectra (Stell & Lightfoot, 1975). Both PR types are depolarised in the dark through opened cGMP-gated channels and release glutamate onto bipolar cells (BCs) and HCs. Through the visual transduction cascade, light-activated visual pigment elicits an intracellular signal amplification pathway resulting in the closure of cGMP-gated channels. This closure leads to membrane hyperpolarisation with cessation of glutamate release, and is termed the "dark current", since glutamate release occurs only in the dark. The mixed rod and cone system of goldfish allows scotopic (intensity-based) and photopic (chromatic) vision spanning from far red to UV wavelengths (Kolb *et al.*, 2001).

Bipolar cells (BCs) and HCs are both second order neurons with cell bodies in the inner nuclear layer (INL). BCs send projections to PRs in the outer plexiform layer (OPL), and meet amacrine cells (ACs) in the INL and inner plexiform layer (IPL), or ganglion cells in the IPL (Euler *et al.*, 2014). HCs have soma residing in the INL and send dendritic projections to PRs in the OPL, but also make contacts with BCs and other cell types (as is discussed later). Goldfish BPs are functionally arranged into an ON/OFF centre-surround antagonistic fields (Kaneko,

1970). ON-centre type experience inhibitory glutamatergic input whereas OFF centre type have excitatory glutamatergic input (Euler *et al.*, 2014). In addition, there are subtypes to the fish BC light response, showing specificity for certain wavelengths of light, likely due to the different input from PRs and HCs (Kato *et al.*, 1991). Light-induced responses of BCs are relayed as graded potentials to sign conserving synapses with ON or OFF centre ganglion cells (GCs) at the IPL, which carry the information to the brain via changing rates of action potential firing. The vertical transmission of signals from PRs to GCs becomes more complex by direct input from HCs or through HC input onto PRs via lateral inhibition (Thoreson & Mangel, 2012).

Figure 1. Diagram of the laminar structure and cellular organisation of the teleost retina. Incident light passes through all retinal layers to trigger electrical responses in photoreceptors (PRs) whose tips extend into the photoreceptor layer (PRL). The tips of PRs are embedded in the retinal pigment epithelium (RPE) which has roles in photo-pigment regeneration and dark adaption. The cell bodies of PRs are located in the outer nuclear layer (ONL), and include both rods and multiple types of cones. PRs synapse with horizontal cells (HC) and bipolar cells (BC) in the outer plexiform layer (OPL). HCs and BCs somas are located in the inner nuclear layer (INL). BCs synapse with amacrine cells (AC) in the INL and ganglion cells (GC) in the inner plexiform layer (IPL). GCs with cell bodies in the ganglion cell layer (GCL) encode information received as action potentials which are transmitted by axons along the optic nerve to visual centres in the brain. Horizontal cells (HC) importantly mediate lateral feedback to PRs as well as feed-forward interactions to PRs and BPs. HCs are also electrically coupled to other HCs of the same physiological type. Shown are two H1 cone HCs (orange) which make non-discriminatory contacts with cones, and are linked to other H1 HCs by gap junctions (*) at their dendritic contacts, as well as their axon terminals. Note rod HCs (shown in red) are axonless. H2 and H3 cells (not shown) contact specific colour cones. Interplexiform cells (IPC) have cell bodies in the INL and send projections to contacts in the IPL and OPL. Müller glial cells (MC) span all retinal layers.

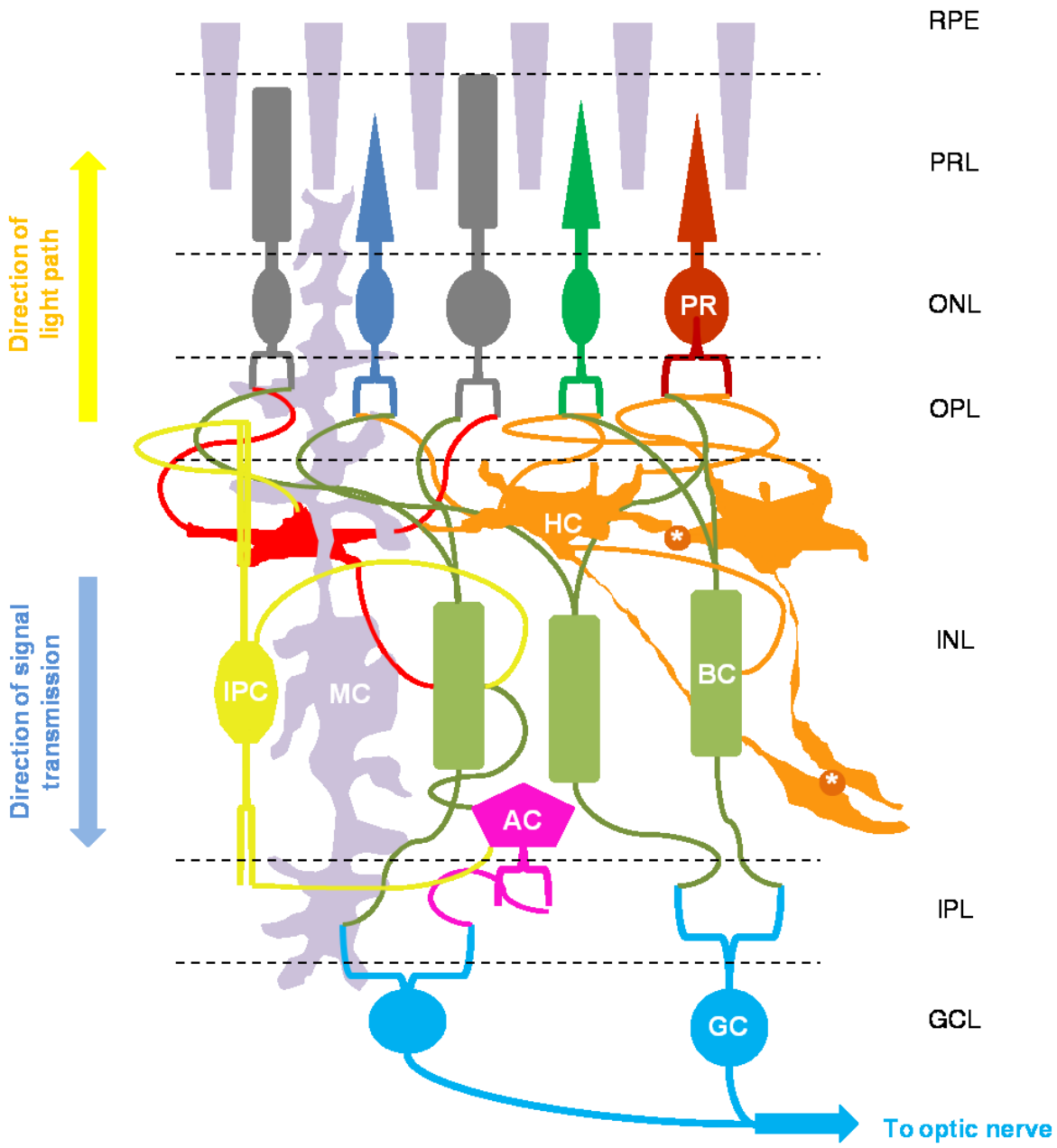
RPE
PRL
ONL
OPL
INL
IPL
GCL
Direction of light path
Direction of signal transmission
PR
HC
IPC
MC
BC
AC
GC
To optic nerve

Amacrine cells (ACs), with cell bodies in the INL are third ordered neurons in the retina, which receive input from BCs and output to GCs; these cells are also organised in an ON-OFF center-surround system (Kato *et al.*, 1991). The goldfish retina possesses an interplexiform cell (IPC) with perikarya in the INL, and processes extending into the OPL and IPL (Kato *et al.*, 1991). In the goldfish, dopaminergic IPCs provide regulation of gap-junction coupling and receptive field size of BP and HCs (Kurz-Isler *et al.*, 1992).

Müller cells (MCs) are the main supportive retinal glial cell, and span the whole retina, providing structural support and extracellular K^+ buffering (Kolb *et al.*, 2001). MCs in all vertebrates are known to mediate re-uptake of glutamate from synaptic clefts (Kolb *et al.*, 2001), modulating post-synaptic excitability through the activity of electrogenic glutamate exchangers (Ishikawa, 2013). MCs may also play a protective role after injury in buffering synaptic glutamate and releasing antioxidants (Lenkowski & Raymond, 2014).

1.2.3 A History of Horizontal Cells - Anatomy to Function

HCs were originally named by the famous neuro-anatomist Santiago Ramón y Cajal (CE 1893) for their place in the retina, stretching horizontally at the OPL (Gallego, 1986). This name bodes well for them as they are also involved in horizontal information transmission and processing. HCs of lower vertebrates have contributed a lot of "firsts" to neurophysiology, being the first vertebrate cell to be recorded intracellularly from above the spinal cord, and the first to show that neurons could respond to stimuli with graded changes in membrane potential as opposed to action potentials (recorded in the teleost retina by Gunnar Svaetichin in 1953) (Piccolino, 1986). Initially, HCs were characterised based on their morphology and anatomical location in the retina, or on their light-evoked responses. Within the retina, HCs broadly respond

to flashes of light with graded hyperpolarisations, which differ with temporal, and spectral sensitivity (Svaetichin & MacNichol, 1959). It was later proposed that this hyperpolarisation was caused by a reduction in excitatory neurotransmitter release from PRs in response to light (Byzov & Trifonov, 1968), eventually revealed to be glutamate.

In 1975, the chromatic responses of all HCs in the goldfish were linked anatomically to four distinct morphological types, then given nomenclature and physiological designations (Stell & Lightfoot, 1975) which persist to the present. These are three axon-bearing cone type HCs, H1, H2, and H3 (in order of their descending location in the INL, and increasing dendritic tree size), and an axon-less rod-type HC (H4). Briefly, all goldfish HCs are of a stellate morphology consisting of a large, flat soma, and extensive processes. Rod HCs cells show a scotopic response, hyperpolarising to all wavelengths of light (Stell & Lightfoot, 1975). Cone type responses can be of luminosity type (hyperpolarising to any wavelength), or show biphasic and even tri-phasic responses to certain wavelengths of light (chromaticity type). The functional distinction between HC types is extended to their receptive field sizes. Goldfish HCs express gap-junctions (GJ) that allow for electrical coupling between other HCs of the same physiological type (e.g. H1 to H1) which results in a laminar syncytia of specific HCs, regulating the sizes of their receptive fields (Gallego, 1986).

Goldfish cone HCs, like in most vertebrates, have long axons with large axon terminals, but unlike in other species these axon terminals do not project to the OPL, but terminate in the INL (Stell, 1975). Interestingly, the same light response from the HC perikaryon can also be recorded from its axon terminal (Weiler & Zettler, 1979), and all axon terminals of the same HC type also form gap junction syncytia (Marshak & Dowling, 1987).

Teleost (and especially goldfish HCs) are useful experimentally as a model retinal neuron given their large size, easy morphological identification in isolation, and well understood membrane properties as described below.

1.2.4 The Inputs and Outputs of HCs

Since early investigations of HC anatomy and light responses, studies have shifted to resolving their mechanistic role in mediating lateral interactions in the retina. Negative feedback to PRs was demonstrated by Baylor in 1971, showing that hyperpolarising current injected into HCs depolarised nearby cones (Piccolino, 1986). Colour-opponency of HCs (hyperpolarising to some wavelengths but depolarising to others) is thought to be mediated by the sum of excitatory input from cones, complexed with the lateral inhibition provided by other HCs onto those cones (Twig *et al.*, 2003). The exact manner by which HCs mediate feedback to PRs is still relatively controversial, but there are a few proposed mechanisms: ephaptic modulation of synapses, GABA-ergic suppression, and pH modulation.

In teleost retinas, the synaptic contacts between HCs and PRs are provided by spinules (tiny dendritic extensions of HCs) which project onto PR ribbon synapses of PRs (Schmitz *et al.*, 1995; Thoreson & Mangel, 2012). HCs are depolarised by PR-released glutamate. Spinule extensions are dynamic, retracting under dark adaption (Raynauld *et al.*, 1979) or glutamate application (Schmitz *et al.*, 1995), and dependent upon Ca^{2+} influx through AMPA-Rs, subsequent increase in $[Ca^{2+}]_i$, causing activation of Ca^{2+}/calmodulin-dependent protein kinase II (CaMKII) (Okada *et al.*, 1999).

The first proposed mechanism of HC feedback was stimulated GABA release from HCs onto PRs. Goldfish HCs are known to produce GABA (Marc, 1982) as well as release it upon

depolarising current injection or glutamate application, and take up GABA when hyperpolarised (Lam & Ayoub, 1983). In addition, some cones express GABA-gated currents. This feedback could only be demonstrated in some HC subtypes, and wasn't found in all species (Twig *et al.*, 2003). For example, in the goldfish retinal, only H1 has been shown to release GABA (Paik *et al.*, 2003).

The second, ephaptic model, proposes that negative feedback occurs by large inward hemichannel currents on HCs, possibly of either Cx of Px type (Fahrenfort *et al.*, 2009; Prochnow *et al.*, 2009). These inward currents would alter the voltage across the HC-cone synapse, and shift the activation of cone $VGCa^{2+}$ channels on the cone pedicle (activation being required for transmitter release) (Kamermans *et al.*, 2001; Fahrenfort *et al.*, 2005).

The third model proposes that H^+ released from cones along with glutamate, or extruded from HCs during normal metabolism, changes synaptic pH, which directly or indirectly modulates cone $VGCa^{2+}$ channels (Vessey *et al.*, 2005). It has also been proposed that this pH mediated mechanism could still be acting through hemichannels (Fahrenfort *et al.*, 2009) or in concert with GABA-ergic signalling (Liu *et al.*, 2013).

In any case, it is clear that the ways by which HCs mediate feedback are complex, and may rely on multiple mechanisms, acting in concert, or becoming differentially influential depending on species, developmental stage, HC subtype, and even illumination state or circadian status (Thoreson & Mangel, 2012). In addition to feedback, HCs also may contribute feed forward information to PRs (Jackman *et al.*, 2011) and BCs (Verweij *et al.*, 1998; Twig *et al.*, 2003; Euler *et al.*, 2014). Though mechanisms of feedback and feed-forward interaction are not universally understood, many of the properties of fish HCs, including their ion channel current profiles, are well documented.

1.2.5 Resting and Excitable Membrane Properties of Retinal HCs

The first study to examine the membrane properties of HCs (catfish) used enzymatic and mechanical isolation to remove all the synaptic inputs that might complicate interpretation of electrophysiological experiments (Johnston & Lam, 1981). This was followed by a whole series of isolated cell experiments, featuring prominently the carp and specifically isolated goldfish HCs. Using electrophysiological methods, isolated goldfish HCs were found to have a resting potential of around -60mV and acted like a K^+ electrode to changing extracellular K^+ ($[K^+]_e$), displaying a non-linear current/voltage relationship due to voltage activation and rectification (elaborated on below) (Tachibana, 1981). These membrane characteristics of isolated HCs are conserved in the intact retina (Byzov & Trifonov, 1981).

Isolated goldfish HCs show action potentials (APs) spontaneously, or in response to supra-threshold current pulses; these APs have an overshoot of 20 mV as well as a plateau potential that lasts for several seconds (Tachibana, 1981). This AP is Ca^{2+}-dependent, and not blocked by tetrodotoxin (TTX) (Tachibana, 1981). Studies have also found the absence of a TTX sensitive current in goldfish HCs *in situ* (Djamgoz & Stell, 1984). Blocking K^+ channels with triethylamine (TEA) results in a prolonged AP, implicating an outward K^+ current in the regulation of APs (Tachibana, 1981). Similar regenerative elements have been found in HCs of other species including catfish (Johnston & Lam, 1981; Lam & Ayoub, 1983; Shingai & Christensen, 1986), and in the common carp (Murakami & Takahashi, 1987, 1988).

1.2.6 Voltage-gated Currents of Isolated Goldfish HCs

The voltage-gated currents responsible for APs in isolated goldfish HCs have been characterised, initially by Tachibana (Tachibana, 1983), and underlie the non-linearity of the

cell's membrane current-voltage relationship. These currents include three K^+ currents, and one Ca^{2+} current. The first K^+ current is Cs^+ sensitive and shows inward rectification, increasing in magnitude with hyperpolarisation from resting potential. The second K^+ current is 4-aminopyridine (4-AP) sensitive, and activated by depolarisation above -25 mV, increasing in magnitude with depolarisation, but inactivates quickly within hundreds of ms. The third is a sustained outward K^+ current that shows TEA sensitivity, was activated by depolarisation beyond -20 mV, showing little inactivation. The VGCa^{2+} current was activated by depolarisation positive to -45 mV and showed maximal conductance at 0 mV, decreasing with further depolarisation. This current was inactivated by increasing $[Ca^{2+}]_i$ (Tachibana, 1983), and also shows sensitivity to intracellular (Dixon *et al.*, 1996) and extracellular (Jonz & Barnes, 2007) acidification. It should be mentioned that isolated fish HCs lose their giant axon (as it is only 1 μM thick) during dissociation protocols. Voltage-dependent currents from isolated axon terminals show the same current identities, but have a total conductance of less than 5% that of the soma (Yagi & Kaneko, 1988).

1.2.7 Glutamate-gated Currents of Isolated Goldfish HCs

Extracellular glutamate elicits an inward current (I_{glu}) both *in situ* and in isolated goldfish HCs (Ishida *et al.*, 1984; Tachibana, 1985; Ishida & Neyton, 1985). I_{glu} can be active at resting potentials after glutamate application over 10 μM, with no significant long term desensitisation; and if in high enough concentration results in AP generation (Ishida *et al.*, 1984). I_{glu} has a reversal potential of around 0 mV, is carried primarily by Na^+, K^+ and Ca^{2+} ions (Tachibana, 1985). It is additionally inhibited by extracellular acidification (Jonz & Barnes, 2007). Teleost HCs are usually thought of as having one main type of iGluR: the AMPA type (Knapp *et al.*,

1990; Huang *et al.*, 2004). The goldfish I_{glu} shows strong Ca^{2+} permeability (Hayashida *et al.*, 1998), indicating that at least some of the AMPA-R expressed are lacking a GluR-2 subunit. Indeed, it was shown immunohistochemically (Peng *et al.*, 1995; Klooster *et al.*, 2001) and pharmacologically (Huang & Liang, 2005) that Ca^{2+}-permeable and impermeable receptors co-exist on isolated goldfish HCs.

1.2.8 Other Membrane Channels of Isolated Goldfish HCs

Carp HCs in the retina are connected in an electrical syncytium with other HCs of the same physiological type (Kato *et al.*, 1991). These can be modulated by dopamine stimulation, which uncouples HCs and reduces gap junction conductance (Teranishi *et al.*, 1983; Lasater & Dowling, 1985) and reduces the size of HC receptive fields (Zucker & Dowling, 1987). Teleost HCs also express functional hemichannels, which in goldfish are the Cx26 type (Kamermans *et al.*, 2001), and known to be inhibited by intracellular (Fahrenfort *et al.*, 2009) and extracellular (Jonz & Barnes, 2007) acidification.

1.2.9 $[Ca^{2+}]_i$ regulation and function in HCs

In goldfish HCs, $[Ca^{2+}]_i$ can be affected by influx from extracellular sources, intracellular buffering, and sequestration or release by intracellular stores. Ca^{2+} enters depolarised HCs via $VGCa^{2+}$ channels (Tachibana, 1983; Yagi & Kaneko, 1988), and iGluRs (if activated by glutamate) (Tachibana, 1985). Goldfish $VGCa^{2+}$ channels are nifedipine sensitive, and show inactivation with increasing $[Ca^{2+}]_i$ (Tachibana, 1983). Teleost HCs possess large $[Ca^{2+}]_i$ buffering capacities (Solessio & Lasater, 2002), as well as caffeine- and ryanodine-sensitive $Ca^{2+}{}_i$ stores capable of Ca^{2+}-induced Ca^{2+}-release (CICR) (Huang *et al.*, 2004; Lv *et al.*, 2014).

There is also some evidence of store-operated membrane Ca^{2+} channels (SOC) that open upon depletion of intracellular stores (Lv *et al.*, 2014). During chronic glutamate application, $VGCa^{2+}$ channels are still active indicating that there are extrusion mechanisms that keep $[Ca^{2+}]_i$ at levels below those which would cause current inactivation (Hayashida *et al.*, 1998). This is done in part by the membrane Na^+/Ca^{2+} exchanger or via the Ca^{2+} ATPase which exchanges $Ca^{2+}{}_i$ with $H^+{}_e$. The interplay of the Na^+/Ca^{2+} exchanger, Ca^{2+} pump, and Ca^{2+} influx allow for HCs to stabilise $[Ca^{2+}]_i$ under chronic depolarisation or glutamate exposure (Hayashida *et al.*, 1998). See Fig 2. for schematic diagram. In addition, oscillatory increases in $[Ca^{2+}]_i$ have been noted in goldfish HCs in response to caffeine application (Lv *et al.*, 2014). Interestingly, spontaneous oscillations in $[Ca^{2+}]_i$ have also been noted in isolated goldfish HCs, although these have not been characterised (Kreitzer *et al.*, 2012).

Whether induced by depolarisation or glutamate, or spontaneously generated, the function of changes in $[Ca^{2+}]_i$ are not well understood in HCs. Ca^{2+} influx through AMPA-Rs is known to be involved in spinule retraction (Schmitz *et al.*, 1995; Okada *et al.*, 1999). In addition, Ca^{2+} through a form of synaptic plasticity may be involved in the regulation of the proportion of Ca^{2+}-permeable and impermeable AMPA-R (Huang & Liang, 2005), as well as affecting GABA release (Kreitzer *et al.*, 2003).

1.3 Model, Thesis Goals, and Hypothesis

1.3.1 The Goldfish Isolated HC as a Model

HCs possess many characteristics that make them labile to hypoxic or ischemic insult, including the expression of glutamate receptors, $VGCa^{2+}$ channels, GJ, and hemichannels.

Figure 2. Diagram of pathways relating to increasing or decreasing $[Ca^{2+}]_i$ in isolated goldfish horizontal cells. (A) Glutamate-activated iGluRs (AMPA-type) open upon ligand binding (green triangle) allowing Ca^{2+}influx. (B) VGCa^{2+} channels open after membrane depolarisation past threshold allowing Ca^{2+} influx. (C) SOC channels may respond to emptying intracellular Ca^{2+} stores, allowing calcium influx. (D) Ryanodine- and caffeine-sensitive channels exist on intracellular Ca^{2+} stores, facilitating CICR. (E) Membrane ATP-powered Ca^{2+} pumps extrude Ca^{2+} in exchange for H^+. (F) Na^+ / Ca^{2+} exchangers couple Na^+ influx to Ca^{2+} efflux. (G) ATP-powered Ca^{2+} pumps facilitate Ca^{2+} uptake into intracellular stores. (H) Intracellular Ca^{2+} buffers help maintain constant levels of $[Ca^{2+}]_i$.

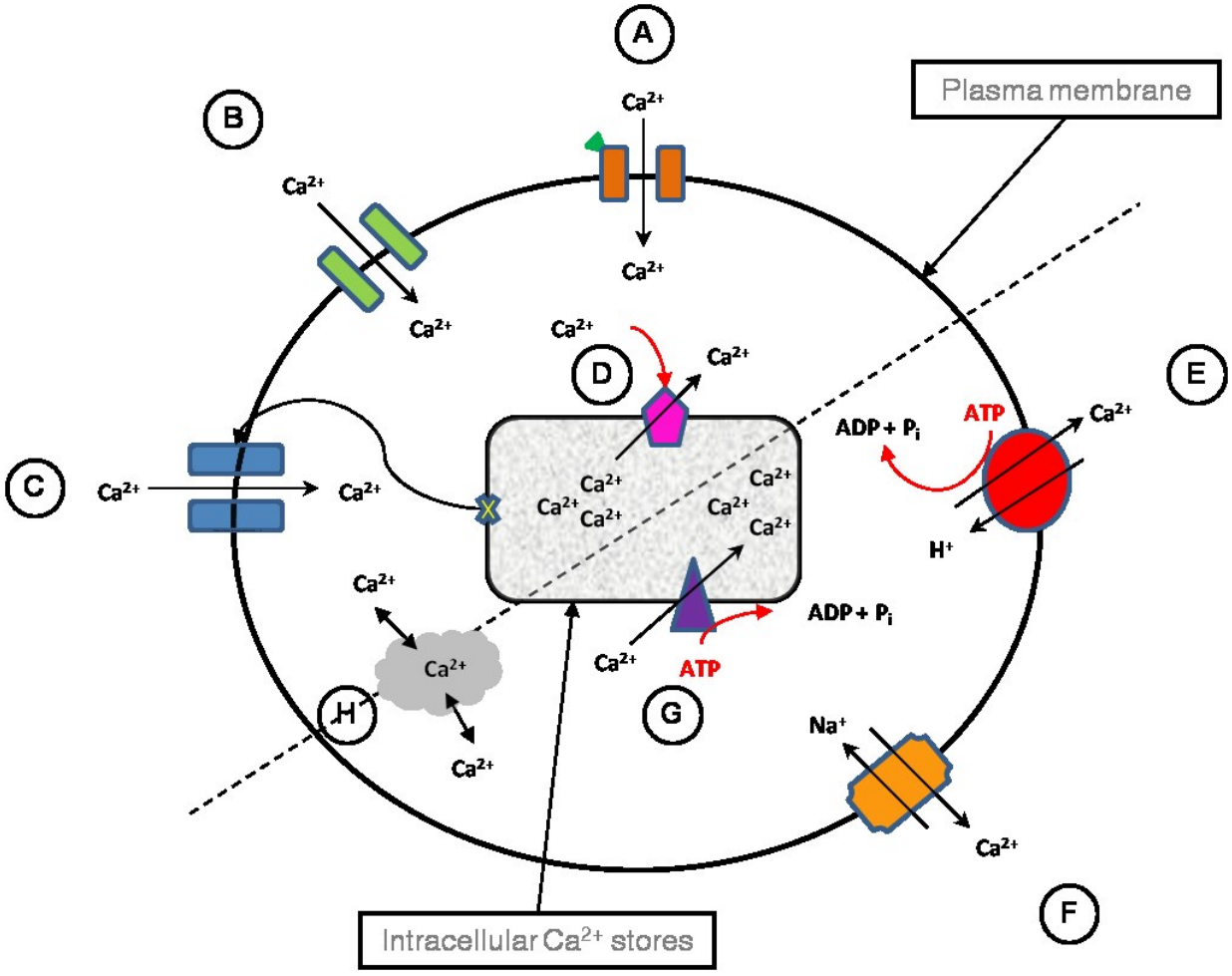
A
B
C
D
E
F
G
H
Plasma membrane
Intracellular Ca2+ stores
Ca2+
ADP + Pi
ATP
H+
Na+

To add insult to injury, HCs are chronically depolarised by glutamate released from PRs under dim illumination. Indeed, INL neurons are usually considered more at risk during retinal hypoxia or ischemia (Osborne *et al.*, 2004). Fish retinal neurons including HCs are labile to glutamatergic injury under normoxic conditions (Villani *et al.*, 1995), but their responses to low O_2 conditions such as ischemia are unknown. As the *Carassius* visual system is electrically suppressed under hypoxia, but functional upon re-oxygenation (Johansson *et al.*, 1997), retinal cells likely undergo some kind of adaptive regulation to avoid low O_2-induced damage and excitotoxicity. Monitoring $[Ca^{2+}]_i$ responses of neurons to insults can demonstrate both adaptive and maladaptive responses, as regulating $[Ca^{2+}]_i$ is critical to cell function and survival (Bickler & Buck, 1998). This can be accomplished using microspectrofluorometric techniques.

1.3.2 $[Ca^{2+}]_i$ Microspectrofluorometry

$[Ca^{2+}]_i$ microspectrofluorometry is the use of fluorescent indicators to monitor $[Ca^{2+}]_i$ in single cells. There are many fluorescent indicators including indo-1, Fura-2, and Fluo-4, each with different fluorescent and Ca^{2+}-binding properties (Grienberger & Konnerth, 2012). Fura-2 is a conjugate of a Ca^{2+} chelating moiety and a fluorescent molecule which changes its excitation peak based on whether the compound is bound or unbound to free intracellular Ca^{2+} (Grynkiewicz *et al.*, 1985). Fura-2 can be excited at 340 (Ca^{2+} bound) and 380 (Ca^{2+} unbound) nm, and emits at 510 nm (Huang *et al.*, 2004). The indicators can be loaded into individual cells by incubation with their membrane-soluble acetoxymethyl ester (AM) form, which allows dye diffusion into the cell; but is then cleaved by intracellular esterases, leaving the impermeable Fura-2 trapped inside (Grienberger & Konnerth, 2012). The ratio of the emission intensity at 510 nm between excitation at 340 and 380 nm allows for monitoring of relative changes in $[Ca^{2+}]_i$.

1.3.3 Objectives and Hypothesis

The goal of this thesis is to better understand possible adaptive responses to energy-limiting conditions in the hypoxia-tolerant goldfish by examining the $[Ca^{2+}]_i$ responses of isolated HCs under conditions of reduced energy availability (ischemia, modeled as OGD). The hypothesis is that in the OGD model of hypoxic and hypoglycemic stress, intrinsic Ca^{2+} dynamics and those elicited by excitatory neurotransmitters will be reduced under OGD, given that increased electrical activity of these cells is directly linked to cell calcium levels, both of which would be expected to be supressed in a tolerant neuron. The primary objective is to characterise the $[Ca^{2+}]_i$ dynamics of isolated HCs using microspectrofluorometric imaging. This will include describing the $[Ca^{2+}]_i$ response of un-stimulated activity (including spontaneous activity), and that induced by glutamate, comparing between normoxic conditions and those under OGD stress. It is predicted that resting $[Ca^{2+}]_i$ will not show an irreversible increase under OGD. It is also predicted that glutamate-elicited increases in $[Ca^{2+}]_i$ (or those that may occur spontaneously) will decrease or remain stable after OGD insult. Determining if and how isolated HCs may regulate their $[Ca^{2+}]_i$ under these conditions will contribute to our understanding of how the retina, and the goldfish as a whole, has adapted to survive conditions of reduced energy availability.

2. Materials and Methods

2.1 Animals

Adult common goldfish (*Carassius auratus*) were obtained from a commercial supplier (AQUAlity Tropical Fish Supply Inc., Mississauga, ON, Canada) and were housed in the University of Ottawa Aquatic Facility where they were maintained for at least two weeks in quarantine to allow for recovery and acclimation to the facility environment. Fish were housed in 170 l tanks fitted with a flow-through system of fresh, aerated, and de-chlorinated City of Ottawa water at a constant temperature of 18 ˚C. Tank photoperiod was kept at a constant light cycle of 12 h light, 12 h dark. Procedures for goldfish care and use were approved by the University of Ottawa Animal Care & Veterinary Services (ACVS) protocol (BL-226) which was implemented in accordance with Canadian Council on Animal Care (CCAC) regulations.

2.2 Isolated HC Preparation

HC isolation closely followed that of Jonz and Barnes (2007). Unless otherwise stated, all reagents and chemicals were sourced from Sigma-Aldrich Canada Co. (Oakville, ON, Canada). Goldfish were dark adapted for approximately 1 h to facilitate the separation of the retina from the RPE. After dark adaptation, fish were stunned with a blow to the head then quickly decapitated and pithed. Eye cups were removed and placed in cold Ca^{2+}-free Ringer's solution (Table I). The sclera and lens were dissected and the whole retina removed from the eye cup and placed in hyaluronidase (100 U ml^{-1}, Cat. No. H-3506) in L-15 solution for 20 min at room temperature. L-15 solution was composed of 70% L-15 media (Leibovitz medium without L-glutamine) and 30% Ca^{2+}-free Ringers. Retinas were washed 3 times for 3 min in fresh L-15 solution and then placed in L-15 solution containing 7 U ml^{-1} papain (Cat. no 3126, Worthington Biochemical Corporation, Lakewood, NJ, USA) for 40 min. Papain was previously activated

with 2.5 mM L-cysteine. Retinas were again rinsed 3 times for 3 min in fresh L-15 solution. Small (~ 4mm^2) sections of retina were removed and mechanically dissociated by repeated, gentle trituration in L-15 solution. The resulting cell suspension was plated onto either glass-bottomed dishes coated with Cell-Tak (Cat. No. 354240, Corning Incorporated, Bedford, MA, USA), or uncoated plastic-bottomed dishes (Corning Inc. Bedford, MA, USA) and allowed to settle and adhere for approximately 15 min before preparing HCs for microspectrofluorometric imaging.

2.3 Relative $[Ca^{2+}]_i$ Measurements

Relative changes in free intracellular Ca^{2+} ($[Ca^{2+}]_i$) were assessed using microspectrofluorometric imaging with the Ca^{2+} indicator Fura-2 (Fura-2-LeakRes-AM; Teflabs, Austin, TX, USA). Isolated cell preparations were protected from light and incubated in normal extracellular solution (ECS, see Table I) containing 5 µM of Fura-2 dissolved in 5 µl DMSO and 0.1% v/v of a 10% w/v Pluronic F-127 solution for 30 min at room temperature to facilitate dye loading. Cells were then washed 3 times in ECS to allow for dye de-esterification and removal of remaining esterified products. Isolated HCs were identified easily from other isolated cell types by their distinguished large flat bodies and thick dendrites (Tachibana, 1983) under low intensity brightfield illumination with a Nikon Eclipse microscope (see Fig. 3 for example). Fluorescent imaging was performed using a Lamda DG-5 wavelength changer (Sutter Instruments, Nocato, CA, USA) to change excitation wavelengths between 340 and 380 nm. Excitation and emission light were passed through a Nikon 40× water-immersion objective lens (numerical aperture 0.80) and emission light was filtered through a 510 nm band pass filter. Fluorescent images at 510 nm were collected with a CCD camera (QImaging, Surrey, BC, Canada) by focusing on a region of

Figure 3. Light micrograph of an isolated goldfish retinal horizontal cell. Isolated horizontal cells (HC) appear with a stellate morphology, with large dendritic processes extending from a large flat soma. A severed HC axon terminal (HCAT) is also shown, HCATs do not remain attached during cell isolation. Bar ~ 100 μm.

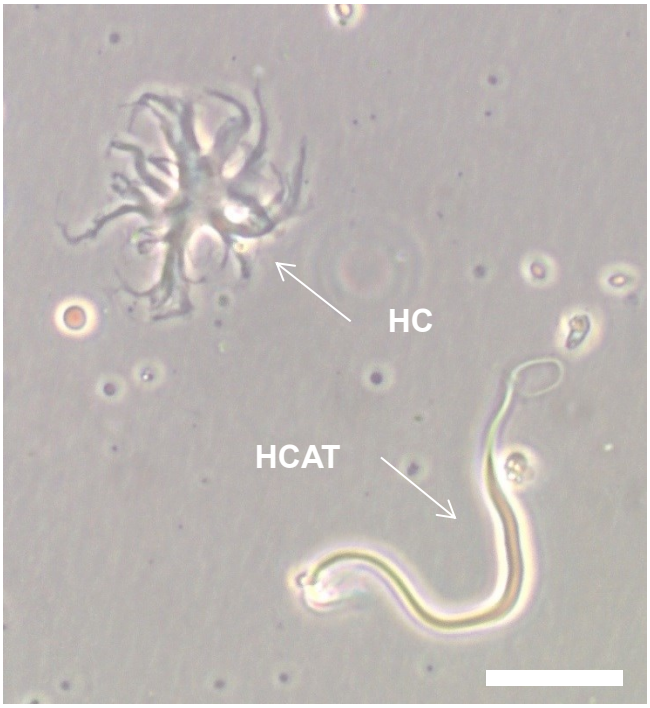
HC
HCAT

interest that encompassed a HC soma. Excitation wavelengths were iteratively changed between 340 and 380 nm, and emission intensity was recorded (500 ms) for both excitation wavelengths every 2 s using Northern Eclipse software (Empix Imaging Inc., Mississauga, ON, Canada). Between exposures during excitation and emission collection cycles light was prevented from contacting the cell by an automated shuttering system. Imaging data was logged in Microsoft Excel (Microsoft Corp., Redmond, WA, USA) using a personal computer

2.4 Experimental Procedures and Solutions

A diamond-shaped perfusion chamber (Warner Instruments Inc, Hamden, CT, USA) was inserted into each Fura-2-loaded culture dish to form a recording chamber. The chamber was continuously perfused at approximately 2 ml min^{-1} by gravity-fed recording solutions held in 60 ml plastic syringes at room-temperature. Recording solution was removed from the recording chamber at the same rate as solution inflow to facilitate continuous bath volume and exchange of solution using a variable-flow pump (Fisher Scientific Canada, Ottawa, ON, Canada). The involvement of Ca^{2+} channels in the generation of spontaneous events or glutamate-induced increases in $[Ca^{2+}]_i$ was tested by perfusing the cell with control ECS solution containing the general Ca^{2+} channel blocker cadmium (Cd^{2+}, 50 μM), the L-type Ca^{2+} channel blocker nifedipine (100 μM, (Lv *et al.*, 2014)), or in Ca^{2+}-free solution containing 1 mM EGTA (Table I). To mimic hypoglycemic conditions for 0 glucose and OGD experiments, 10 mM glucose was replaced with equimolar sucrose (Thompson *et al.*, 2006; Dvoriantchikova *et al.*, 2012). During OGD experiments, the pO_2 of solutions was lowered by bubbling the ECS reservoir with 100% nitrogen gas to displace dissolved O_2 (Wilkie *et al.*, 2008). Control solutions were bubbled with compressed air.

Table I: Ringer's and extracellular recording solutions (ECS) composition. In all solutions, pH was adjusted to 7.80 with NaOH.

		Extracellular Recording Solutions (mM)			
Reagent	Ca^{2+}-free Ringers	Control solution	Ca^{2+}-free	Cd^{2+}-blocking	OGD/0 glucose
NaCl	120	120	120	120	120
KCl	2.6	5	5	5	5
$CaCl_2$	-	2.5	-	2.5	2.5
$MgCl_2$	-	2	3.5	2	2
Glucose	10	10	10	10	-
Sucrose	-	-	-	-	10
HEPES	10	10	10	10	10
NaH_2PO_4	0.5	-	-	-	-
EGTA	-	-	1	-	-
$CdCl_2$	-	-	-	0.05	-

Raw traces from imaging experiments are presented as arbitrary units (A.U.) of the ratio of fluorescence emission intensity after excitation with 340 nm and 380 nm ($R_{340/380}$). Parameters chosen to describe each spontaneous event included event duration, time to peak from baseline level, amplitude, area under the curve (AUC), and frequency. Events were analysed using OriginPro 2015 (OriginLab Corp. Northampton, MA, USA) built in peak analysis algorithm which reliably identifies the start, end, and peak values, as well as the AUC of spontaneous events. Duration was measured as the time (s) between the start and end of each event. Time to peak (TTP) was the time (s) between the start of the event and the peak amplitude of that event. Amplitude was measured as the difference between the peak value and averaged baseline before and after that event. AUC was calculated as the integral of amplitude over time of each event using OriginPro 2015. Frequency was measured as the number of events per time period (5 min) of observation. For amplitude and AUC measurements, values were scaled to the largest

magnitude event for each experiment (Lv *et al.*, 2014) due to high variability between cells. Glutamate-elicited events were analysed for peak and steady state amplitude in the same manner as spontaneous events.

For experiments that tracked changes in spontaneous or elicited events over time (sham), or under conditions of OGD or 0 glucose, data were compared using a non-parametric repeated measures Friedman's test with appropriate multiple comparisons *post hoc* tests. When comparing two paired groups, a Wilcoxon signed rank text was employed. Grouped analyses were carried out using GraphPad Prism 5 (Graphpad Software Inc., San Diego, CA, USA). Normality tests on data were performed using a Shapiro-Wilk or D'Agostino K-squared test with OriginPro 2015 (OriginLab Corporation, Northampton, MA, USA). Occasionally, spontaneous increases in Ca^{2+} would occur but not resemble the typical phenotype of the vast majority of spontaneous events (e.g. duration was extremely long, may have represented a change in baseline calcium concentration), these increases were not considered in the analysis for OGD, 0 glucose, or sham experiments. Figures were generated using Excel 2007 (Microsoft Corp.) for raw trace presentation or OriginPro 2015 for histogram and grouped data plots.

3. Results

3.1 Variability in Recording $[Ca^{2+}]_i$ in Isolated HCs

Initial observations of relative $[Ca^{2+}]_i$ dynamics of HCs using microspectrofluorometric techniques revealed several interesting phenotypes including differences in stable baseline values as well as the occurrence of spontaneous $[Ca^{2+}]_i$ events. For the purpose of this thesis, spontaneous events are defined as transient increases in $[Ca^{2+}]_i$ that are distinct from background noise and which cannot be attributable to external stimuli (e.g. glutamate application). Two main phenotypes of calcium activity were observed (Fig. 4A). These were either cells that displayed spontaneous $[Ca^{2+}]_i$ events, while maintaining a stable baseline from the start of recording, or were cells that switched between a state of non-responsiveness with elevated baseline $[Ca^{2+}]_i$ to a lower stable baseline with spontaneous events. Very rarely, some cells did not display any spontaneous events during the course of observation. No correlation between these three response phenotypes and morphological characteristics of isolated HCs was determined. A change from an elevated baseline to a lowered baseline occurred spontaneously (Fig. 4A) or could be induced by transient bath application of 100 μM glutamate (Fig. 4B). In 24/25 cells tested where the cell was initially in an elevated baseline state, glutamate application further increased $[Ca^{2+}]_i$ to a higher steady level, and upon washout, the $[Ca^{2+}]_i$ baseline dropped to a new lowered steady state, below initial levels.

Figure 4. Spontaneous activity and $[Ca^{2+}]_i$ dynamics in isolated horizontal cells. (A) Representative traces of different phenotypes of $[Ca^{2+}]_i$ changes in HCs during perfusion with normal ECS. **(B)** Representative trace showing effect of transient bath-applied glutamate (100μM, bar) on elevated baseline $[Ca^{2+}]_i$ (n=24 cells). **(C)** Effect of transient bath-applied glutamate (100 μM, bar) on spontaneous events of long duration (n=4 cells). All traces: values presented are arbitrary units (A.U.) of the Fura-2 emission ratio 340 nm/380 nm. An increase in the ratio represents a relative increase in $[Ca^{2+}]_i$ and vice versa.

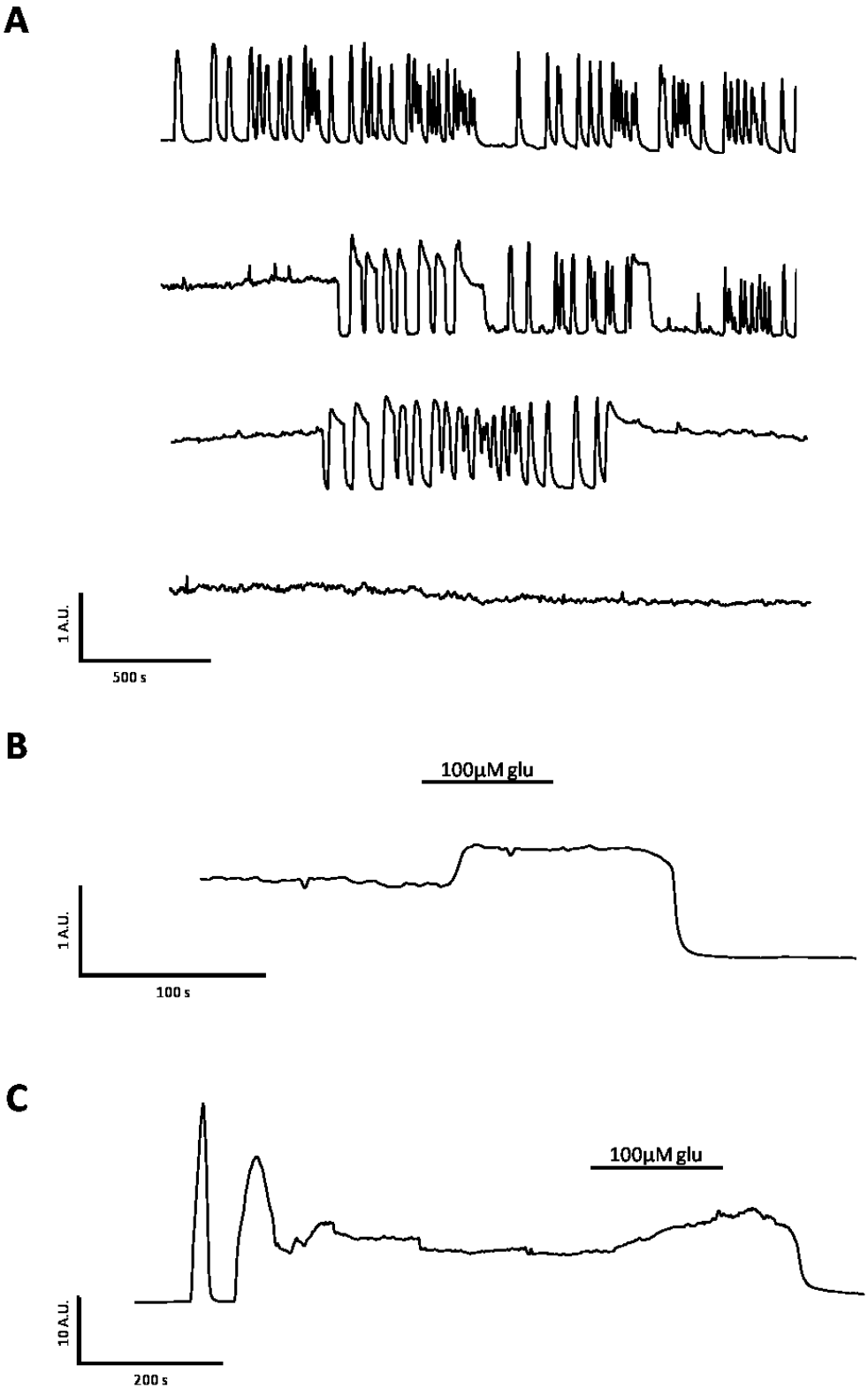
A
1 A.U.
500 s
B
100µM glu
1 A.U.
100 s
C
100µM glu
10 A.U.
200 s

3.2 Spontaneous $[Ca^{2+}]_i$ Events

Spontaneous $[Ca^{2+}]_i$ transients in isolated fish HCs have been noted (Kreitzer *et al.*, 2012) but not characterised. Spontaneous $[Ca^{2+}]_i$ activity was recorded in 86% of 135 cells from 78 goldfish tracked for <15 min without treatment. All cells tracked for over 15 min showed spontaneous events. Most spontaneous events displayed a characteristic peak, eventually recovering to the baseline $[Ca^{2+}]_i$ within 40 s after onset. Occasionally (< 5% of events), extended spontaneous events (lasting longer than 40 s) occurred and in addition to a transient peak, showed an extended plateau phase that recovered spontaneously. These events could be made to recover to baseline with transient bath application of 100 μM glutamate (n=4, Fig. 4C).

Spontaneous event characteristics varied within and between cells. To get a better sense of this variation, data from individual spontaneous events (n=5 cells from 5 different fish) where spontaneous activity was tracked for at least 30 un-interrupted min were pooled, and these data were analysed for several characteristics (see Methods). Frequency distributions from 5 cells are presented in Figure 5 and illustrate the following parameters: event duration, time to peak, amplitude, area under the curve (AUC), and event frequency. Summary statistics for these data are presented in Suppl. Table I and II. The duration of spontaneous events in this pooled population was varied, the majority (96%) lasted between 8 and 44 s (Fig. 5A). Few events (4%) lasted longer than 50 s, and these long events showed a transient peak followed by an elevated steady state (e.g Fig. 4C). The rise time (time to peak) of each event occurred for the most part within a narrow range (Fig. 5B) of 4 to 12 s. The events' amplitude and AUC (Fig. 5C D) showed skewed, uni-modal peak distributions unlike those for event frequency (Fig. 5E). All parameters varied significantly between cells (see Suppl. Table II). Due to the acquisition procedures (see Methods), temporal resolution was limited to time periods of 2 s.

Figure 5. Frequency distributions of spontaneous event parameters in isolated horizontal cells. Data pooled from n=5 cells from different fish with activity tracked over 30 min in normal solution. **(A)** Distribution of duration of spontaneous events, n=279 events, for display purposes values over 100 (n=3 events) are not shown. **(B)** Distribution of time of rise from base to peak amplitude. **(C)** Distribution of amplitudes of spontaneous events. **(D)** Distribution of the area under the curve (AUC, integrated amplitude over time) of spontaneous events. **(E)** Distribution of frequency of event occurrence in subsequent 5 min time periods within each cell, n=40 periods. All panels: for summary descriptive statistics see Suppl. Table. I and for inter-cell comparison of means see Suppl. Table. II.

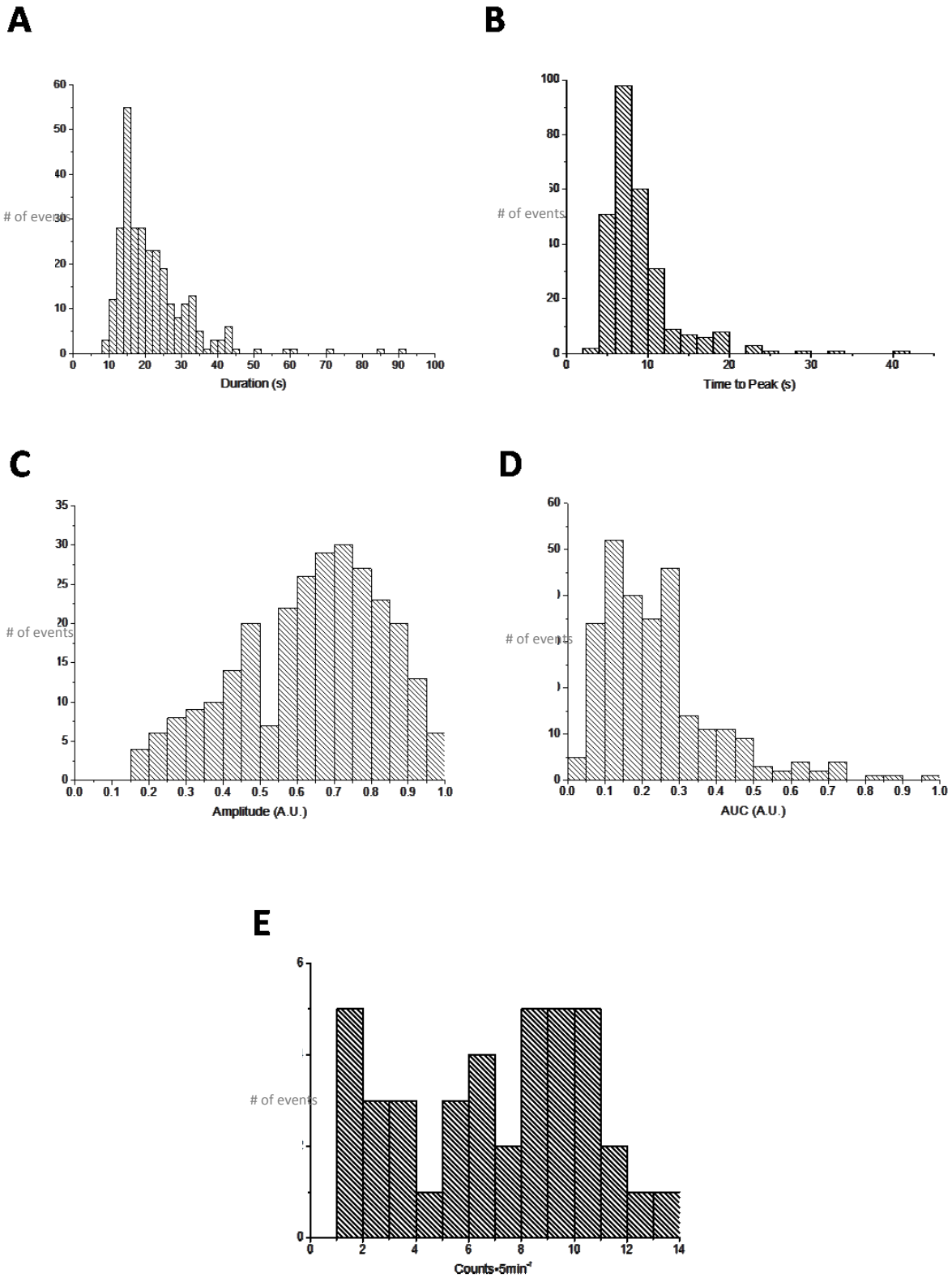
A
# of events
Duration (s)
B
# of events
Time to Peak (s)
C
# of events
Amplitude (A.U.)
D
# of events
AUC (A.U.)
E
# of events
Counts•5min⁻¹

3.3 Spontaneous Event Generation Requires External Ca^{2+}

Stimulated and spontaneous Ca^{2+}-dependent action potentials (APs) have been noted in isolated fish HCs, and involve Ca^{2+} influx from extracellular sources (Tachibana, 1981; Murakami & Takahashi, 1988; Takahashi *et al.*, 1993) which may account for the spontaneous Ca^{2+} events observed. To determine the source of Ca^{2+} mediating spontaneous events, extracellular Ca^{2+} (Ca^{2+}_e) was removed by replacement of bath perfusate with 0 mM Ca^{2+} ECS supplemented with EGTA (see Table I for composition). Figure 6A shows that transient removal of Ca^{2+}_e resulted in elimination of spontaneous activity (SA) and could be achieved multiple times in the same cell with full recovery upon re-application of normal ECS. Interestingly, re-application of Ca^{2+}_e resulted in an initial persistent elevation of $[Ca^{2+}]_i$ that eventually recovered to pre-treatment baselines along with the re-immergence of SA (n=2 cells, see Fig. 6A). During periods where Ca^{2+}_e was removed, there was never any SA (n=18 cells, data not shown). These data indicated that Ca^{2+} influx from extracellular sources may be required for SA generation.

As Ca^{2+}_e is required for SA, determining the source of Ca^{2+} influx was achieved through blockade of L-type Ca^{2+} channels, thought to be the major $VGCa^{2+}$ channel in goldfish HCs (Tachibana, 1983; Huang & Liang, 2005). Blockade of Ca^{2+} influx through $VGCa^{2+}$ channels using the external blocking agents of Cd^{2+} (50 μM) and nifedipine (100 μM) was tested in the presence of 2.5 mM Ca^{2+} perfusate. Extracellular Cd^{2+} (50 μM) reversibly eliminated spontaneous activity (n=3, Fig. 6B) and was achieved twice with full recovery in all cells tested (n=2 cells). Nifedipine (100 μM) also eliminated spontaneous activity (Fig. 6C), which did not recover upon removal of nifedipine solution (n=4).

Figure 6. Spontaneous activity requires influx of Ca^{2+} from extracellular sources. (A) Removal of extracellular Ca^{2+} (bar) reversibly eliminates spontaneous events (n=2). Note the persistent elevation of $Ca^{2+}{}_i$ upon replacement of extracellular Ca^{2+} in the perfusate. **(B)** 50 μM Cd^{2+} (bar) application reversibly eliminates spontaneous events (n=3). **(C)** 100 μM nifedipine application (bar) eliminates spontaneous events (n= 4, no recovery). All traces: values presented are arbitrary fluorescent units of the fura-2 emission ratio 340 nm/380 nm, an increase in the ratio represents an increase in $[Ca^{2+}]_i$.

A

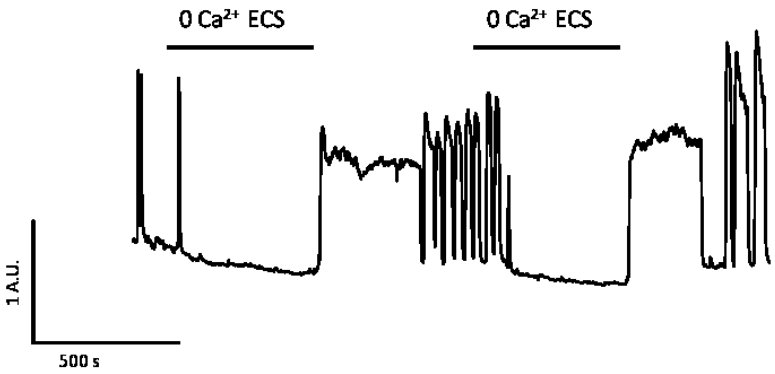
0 Ca2+ ECS
0 Ca2+ ECS
1 A.U.
500 s

B

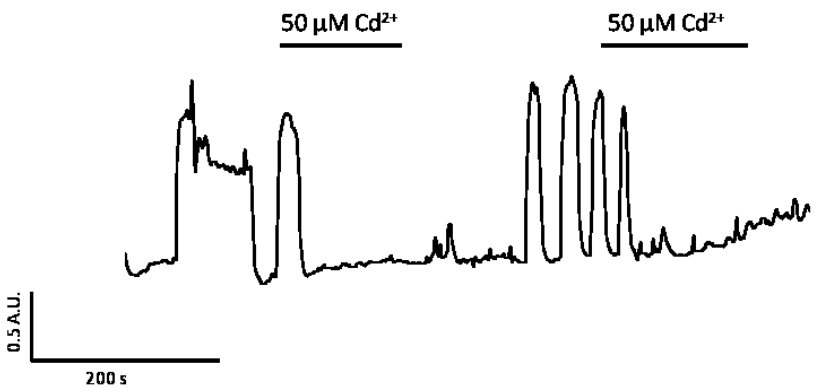
50 µM Cd2+
50 µM Cd2+
0.5 A.U.
200 s

C

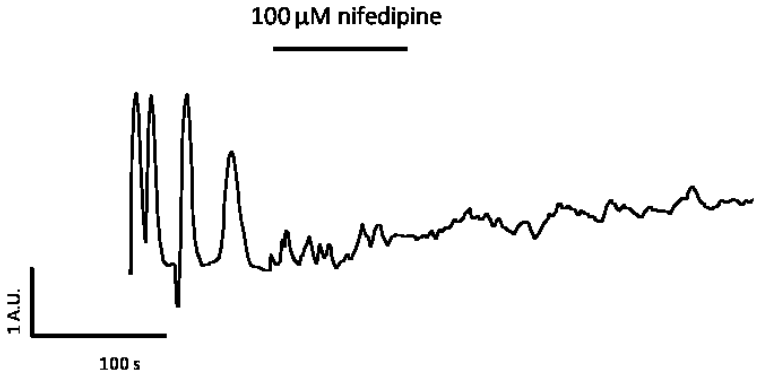
100 µM nifedipine
1 A.U.
100 s

3.4 Effects of Oxygen-Glucose Deprivation on Spontaneous Ca^{2+} Activity

Regulating increases in $[Ca^{2+}]_i$ during conditions of low O_2 and substrate availability may be adaptive. The SA of HCs was tracked before, during and after exposure to oxygen-glucose deprivation (OGD, a model of ischemia). Spontaneous activity was reduced in amplitude after 15 min of OGD treatment, without recovery upon washout (n= 10 cells, Fig. 7A). Figure 7B shows a close-up of exemplar spontaneous events from before, during, and after OGD, demonstrating that both amplitude and the AUC are reduced after OGD. Average metrics of the last one or two spontaneous events from 5-min periods directly before OGD, during the last 5 min of OGD, and after 5 min of OGD removal were compared (Fig. 8 A-D). Event amplitude fluorescence intensity decreased by 50% or from 0.98 to 0.50 A.U. and did not recover. The magnitude of the AUC of spontaneous events also decreased from control values, by over 50% from 0.88 to 0.40. The % decrease in fluorescent intensity may not correspond to an equivalent % decrease in absolute $[Ca^{2+}]_i$, requiring calibration to known the extent of the concentration change. Frequency of event occurrence, event duration, and the time from baseline to peak did not change between conditions ($p>0.05$, Friedman's test). Average relative baseline $[Ca^{2+}]_i$ measurements were also taken for the same time periods as the other metrics and compared (Fig. 7F). There was no significant difference ($p>0.05$, Friedman's test) between treatments suggesting that OGD did not induce increases in baseline $[Ca^{2+}]_i$. In sham experiments, in which cells were superfused with normal ECS over identical periods of time, no significant differences in any metric, with the exception of baseline measurements which showed a small, significant decrease in baseline between control and post-application values (Suppl. Fig. 1, statistical comparison found in Suppl. Table VI).

Figure 7. Phenotypes of HC $[Ca^{2+}]_i$ dynamics under acute OGD. (A) A representative trace showing spontaneous activity observed under treatment with 20 min of OGD (bar). **(B)** Enlarged spontaneous events from (A) showing representative transients from the 5 min before OGD onset (control), during the last 5 min of OGD (OGD), and after 5 min after OGD washout (Post-application). All traces: values presented are arbitrary fluorescent units of the fura-2 emission ratio 340 nm/380 nm, an increase in the ratio represents an increase in $[Ca^{2+}]_i$.

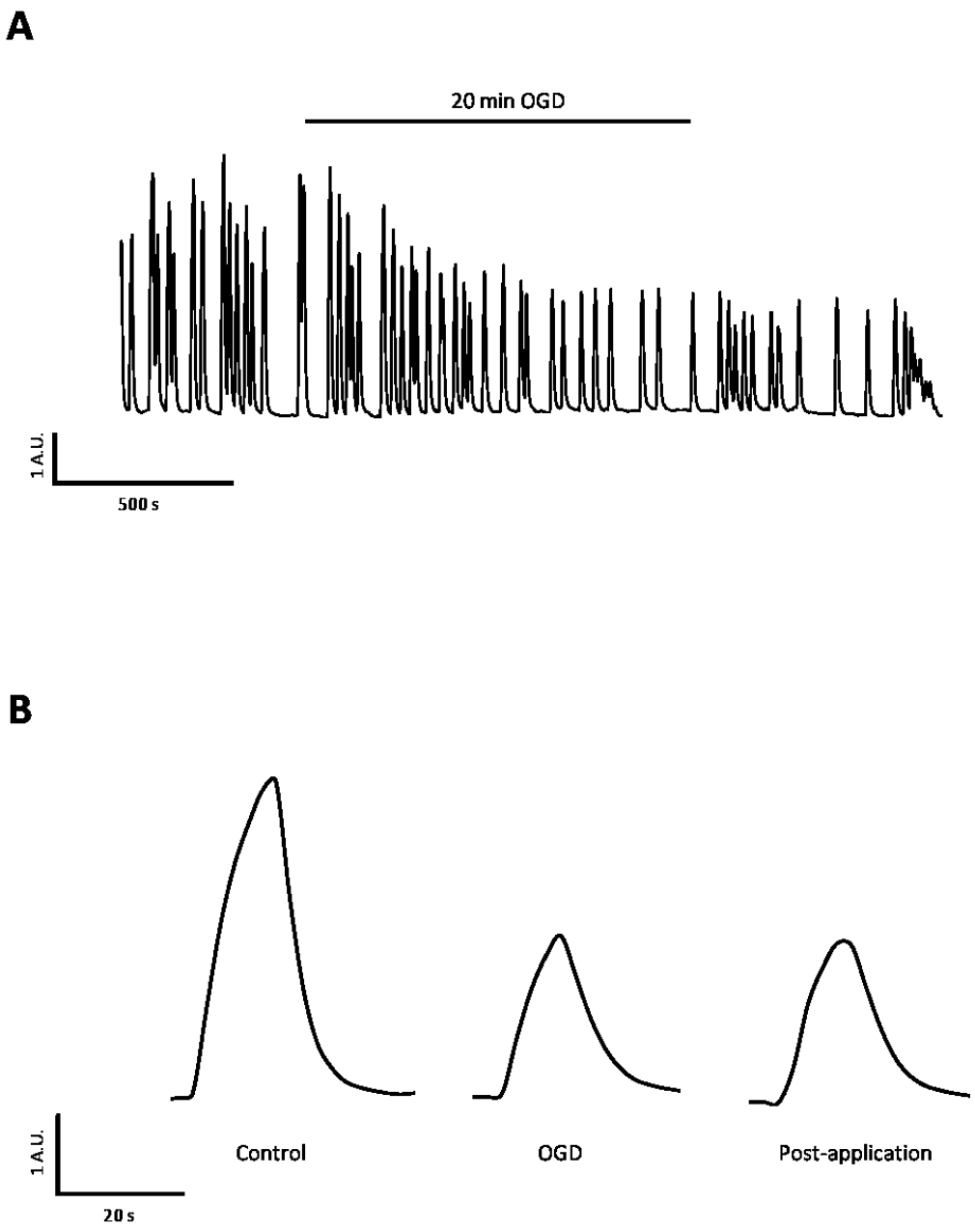
A
20 min OGD
1 A.U.
500 s
B
1 A.U.
20 s
Control
OGD
Post-application

Figure 8. Summary of effects of OGD treatment on spontaneous events. Values taken from 5 min before the onset of OGD (Control), during the last 5 min of OGD (OGD) and for the 5 min after the cell had time to recover in control solution for 5 min (Post-application). **(A)** Duration of spontaneous events (s)**. (B)** Time to peak (s). **(C)** Amplitude of spontaneous events (A.U.). **(D)** Area under the curve (AUC, integrated amplitude over time). **(E)** 5 min event frequency (counts/5 min). **(F)** Baseline [Ca^{2+}]. For all comparisons, significant difference from initial control values are presented with asterisk (*) (Friedman's with Dunns post-test ($p<0.05$), n= 10. Means (red bars). All panels: statistical summary presented in Suppl. Table III.

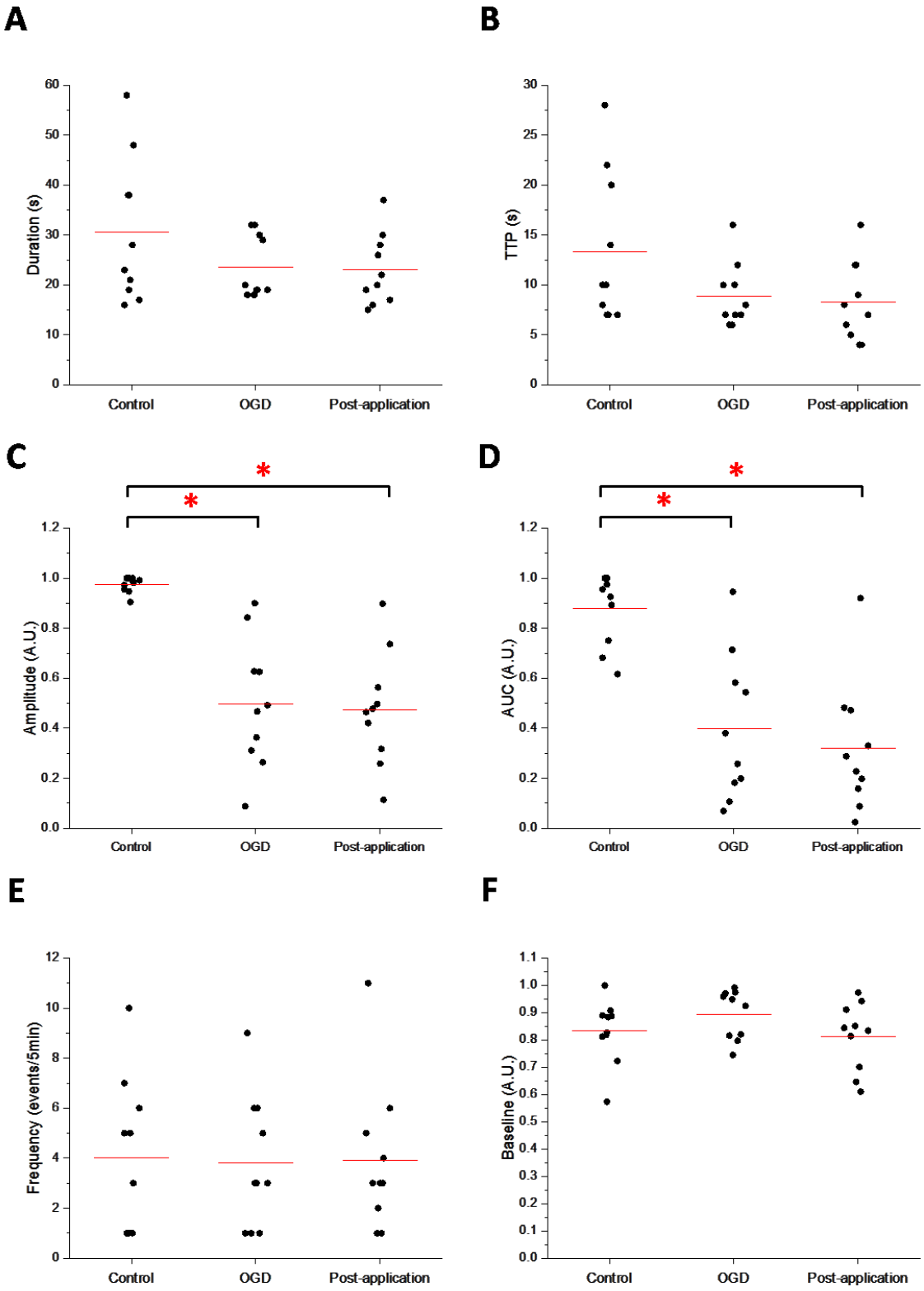
A
Duration (s)
0
10
20
30
40
50
60
Control
OGD
Post-application
B
TTP (s)
0
5
10
15
20
25
30
Control
OGD
Post-application
C
*
*
Amplitude (A.U.)
0.0
0.2
0.4
0.6
0.8
1.0
1.2
Control
OGD
Post-application
D
*
*
AUC (A.U.)
0.0
0.2
0.4
0.6
0.8
1.0
1.2
Control
OGD
Post-application
E
Frequency (events/5min)
0
2
4
6
8
10
12
Control
OGD
Post-application
F
Baseline (A.U.)
0.0
0.1
0.2
0.3
0.4
0.5
0.6
0.7
0.8
0.9
1.0
1.1
Control
OGD
Post-application

To separate possible contributing factors of both O_2 and glucose removal during OGD experiments on reducing spontaneous event amplitude and AUC, a similar set of experiments was completed that included the removal of glucose only, while maintaining normoxic conditions (Figs 9-10). Under these conditions, SA showed a reduction in amplitude and AUC without recovery, and subsequent irreversible increases in baseline $[Ca^{2+}]_i$ (Fig. 9A). Figure 9B shows expanded representative transients from before, during, and after 0 glucose treatments. Following glucose removal, both event amplitude and AUC were reduced, and eventually SA was eliminated following an irreversible elevation of baseline $[Ca^{2+}]_i$. Average metrics of the last one or two spontaneous events from 5 min periods directly before 0 glucose treatment and during the last 5 min of 0 glucose treatment were compared for event duration, time to peak, amplitude, and AUC (n=6 cells, Fig. 10A-D). With the exception of frequency and baseline parameters, a post-application time point could not be adequately compared because the resulting elevated baseline eliminated spontaneous event generation (e.g. Fig. 9B). Metrics for event frequency and $[Ca^{2+}]$ baseline levels (Fig.10 E-F) were compared for 5-min periods directly before 0 glucose treatment, during the last 5 min of 0 glucose treatment, and in the 5 min following 5 min re-introduction of normal glucose conditions in recording solution (Post-application).

Like with OGD treatment, there was no significant difference in spontaneous event duration or time to peak (Fig. 10A,B) as compared between the control and 0 glucose conditions (n=6, Wilcoxon, $p>0.05$). Average event amplitude fluorescent intensity (Fig. 10C) was significantly decreased from 0.94 to 0.50 A.U. between control and 0 glucose conditions (Wilcoxon test, $P<0.05$). Average event AUC was also similarly decreased from an initial value of 0.93 to 0.45 (Fig. 10D). Similar to OGD treatment, there was no significant difference between control and 0 glucose conditions for frequency (Fig. 10E, $p>0.05$ Friedman's test with

Figure 9. Phenotypes of HC [Ca^{2+}] dynamics displayed following acute removal of glucose. **(A)** Representative trace showing reduced spontaneous Ca^{2+} activity observed under 0 glucose treatment with and subsequent elevation of Ca^{2+} baseline. **(B)** Enlarged spontaneous events from (A) showing representative transients from the 5 min before 0 glucose onset (control), during the last 5 min of 0 glucose (0 glucose), and after 5 min after 0 glucose washout (Post-application). All traces: values presented are arbitrary fluorescent units of the fura-2 emission ratio 340 nm/380 nm, an increase in the ratio represents an increase in $[Ca^{2+}]_i$.

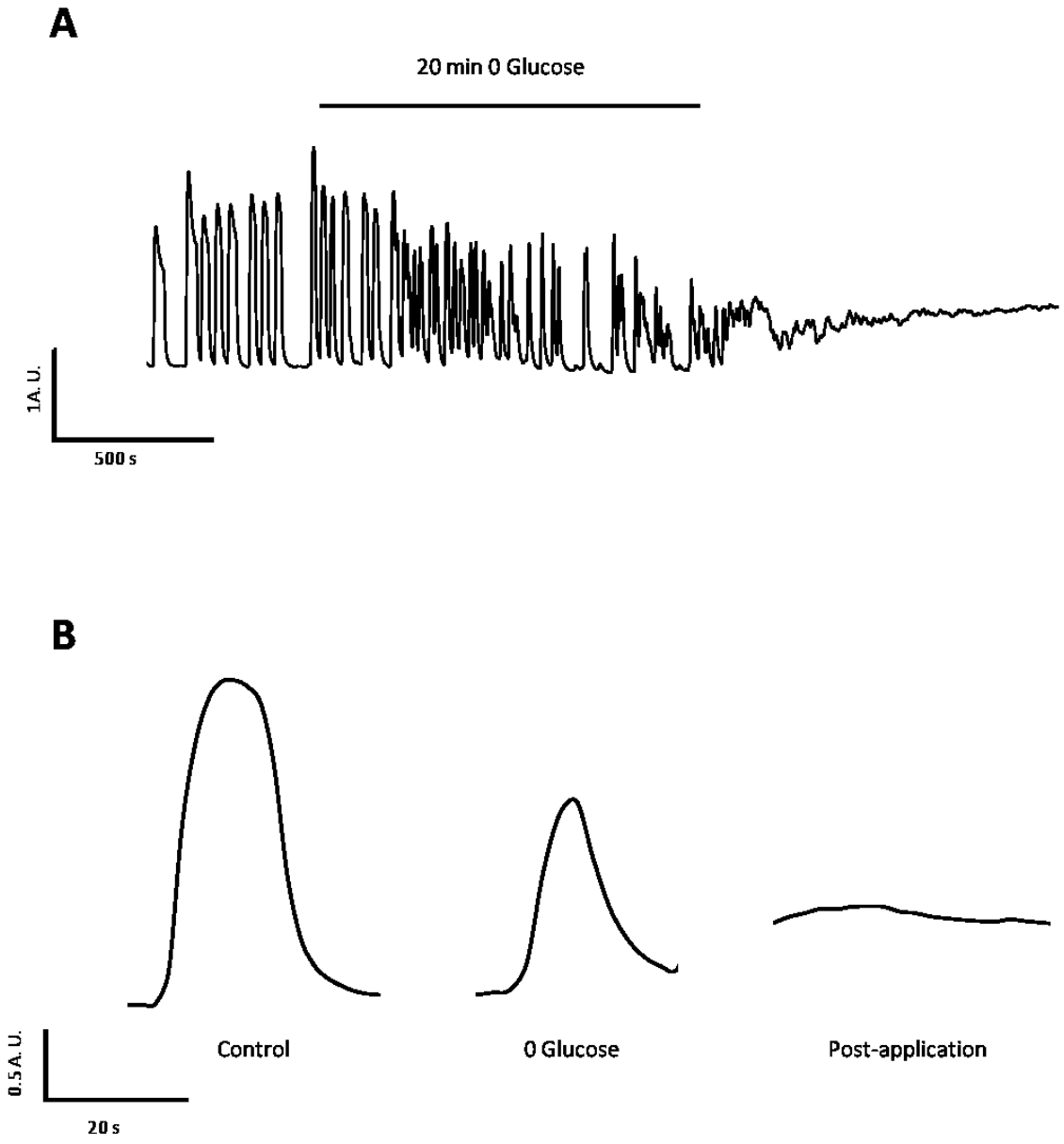
A
20 min 0 Glucose
1A. U.
500 s
B
0.5A. U.
20 s
Control
0 Glucose
Post-application

Figure 10. Summary of effects of glucose removal on spontaneous Ca^{2+} events. Values taken from 5 min before the onset of 0 glucose (Control), during the last 5 min of 0 glucose and for the 5 min after the cell had time to recover in control solution for 5 min (Post-application). **(A)** Duration of spontaneous events (s)**. (B)** Time to peak (s). **(C)** Amplitude of spontaneous events (A.U.). **(D)** Area under the curve (AUC, integrated amplitude over time). **(E)** 5 min event frequency (counts/5 min). **(F)** Baseline [Ca^{2+}]. For panels A-D, significant differences are marked with an asterisk (Wilcoxon, $p<0.05$) n=6; for panels E-F, significant differences are indicated with an asterisk (*) (Friedman's with Dunns post-test ($p<0.05$), n= 8. Means (red bars). All panels: statistical summary presented in Suppl. Table IV and V.

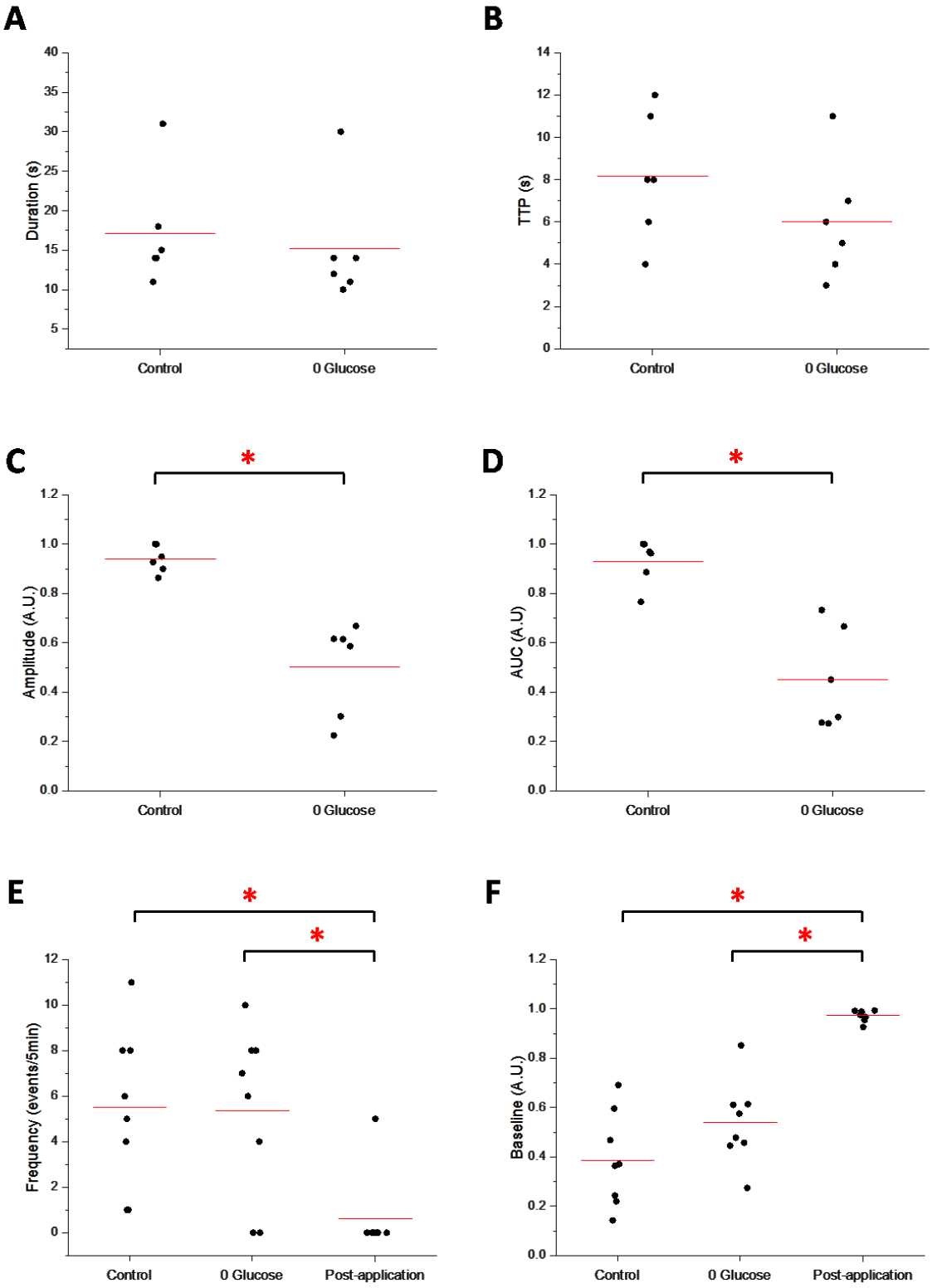
A
Duration (s)
40
35
30
25
20
15
10
5
Control
0 Glucose
B
TTP (s)
14
12
10
8
6
4
2
0
Control
0 Glucose
C
*
Amplitude (A.U.)
1.2
1.0
0.8
0.6
0.4
0.2
0.0
Control
0 Glucose
D
*
AUC (A.U)
1.2
1.0
0.8
0.6
0.4
0.2
0.0
Control
0 Glucose
E
*
*
Frequency (events/5min)
12
10
8
6
4
2
0
Control
0 Glucose
Post-application
F
*
*
Baseline (A.U.)
1.2
1.0
0.8
0.6
0.4
0.2
0.0
Control
0 Glucose
Post-application

Dunn's post-test), but there was a difference between the first two conditions and the post-application time point, namely because an elevated baseline precluded the generation of spontaneous events. Contrary to the results shown in Fig. 8F where baseline values were unchanged by OGD treatment, there was a clear increase in baseline values in all cells tested with 0 glucose treatment (Fig. 10E). This increase was from 0.39 to 0.97 A.U. and significant as determined by a Friedman's test ($P<0.05$) between control and post-application conditions, as well as between 0 glucose treatment and the post-application condition (Dunn's post test $P< 0.05$). This increase in baseline calcium may represent a loss in the cell's ability to regulate its $[Ca^{2+}]_i$ under conditions of low glucose.

3.5 HCs Show Stereotyped $[Ca^{2+}]_i$ Responses to Glutamate Application

HCs are known to respond to glutamate application with membrane depolarisation and increased $[Ca^{2+}]_i$ via influx through both glutamate receptors, and subsequently $VGCa^{2+}$ channels (Hayashida *et al.*, 1998). The effects of glutamate on isolated goldfish HCs in the present study were tested with transient bath application of 100 μM glutamate (Fig. 11 A), a saturating dose that does not cause significant de-sensitisation (Tachibana, 1985). The $[Ca^{2+}]_i$ response of HCs to glutamate application was typical and involved an initial increase in $[Ca^{2+}]_i$ to a peak amplitude, a decay to an elevated plateau phase that persisted for as long as glutamate was applied, and recovery to baseline levels after glutamate washout (Fig. 11 B). This response could be repeated multiple times in the same cell. The onset of the glutamate response was limited only by bath perfusion rate. In a small set of experiments in which a fast-step microperfusion system was used to apply glutamate, onset of the glutamate response was immediate (Data not shown).

Figure 11. Effects of transient glutamate (100 µM) application on $[Ca^{2+}]_i$ in isolated HCs. **(A)** Representative trace shows typical response of HCs to transient glutamate application. An initial-glutamate induced transient increase in $[Ca^{2+}]_i$ decays to a sustained rise in $[Ca^{2+}]_i$ that persists for the duration of glutamate application and recovers with glutamate removal. Values presented are arbitrary fluorescent units of the fura-2 emission ratio 340 nm/380 nm, an increase in the ratio represents an increase in $[Ca^{2+}]_i$. **(B)** Diagram of the glutamate response components displaying the different amplitudes (red arrows) of the transient peak, as well as the steady state increase in $[Ca^{2+}]_i$.

A

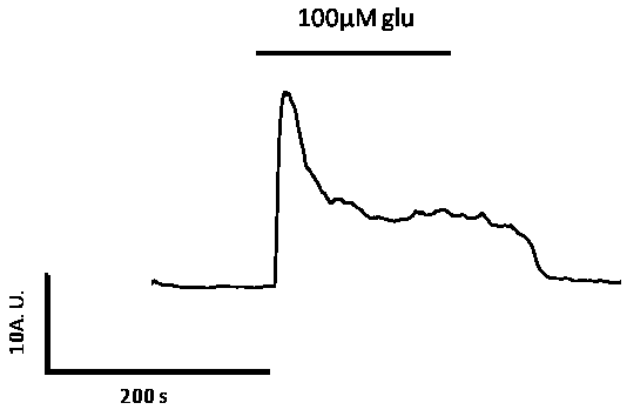

B

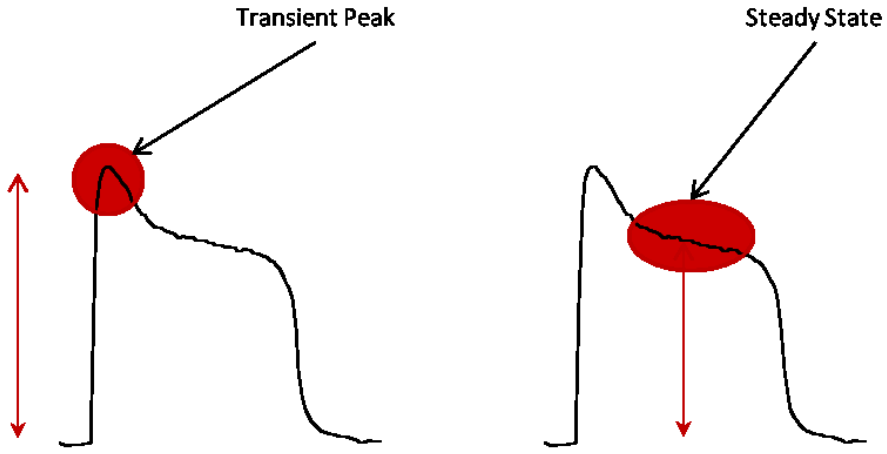

3.6 Glutamate-elicited $[Ca^{2+}]_i$ Responses Require External Ca^{2+}

The cellular $[Ca^{2+}]_i$ response to glutamate and involvement of nifedipine-sensitive pathways has been previously demonstrated in fish HCs (Hayashida *et al.*, 1998). To better understand the mechanisms governing modulation of the $[Ca^{2+}]_i$ response to glutamate, Ca^{2+} was removed from the extracellular perfusate to verify the involvement of Ca^{2+}_e (Fig. 12A). Removal of Ca^{2+}_e eliminated glutamate-elicited increases in $[Ca^{2+}]_i$, regardless of whether Ca^{2+}_e was removed before or during glutamate application (n=6 cells). The glutamate-mediated increase in $[Ca^{2+}]_i$ may involve Ca^{2+}_e influx through glutamate receptors and/or $VGCa^{2+}$ channels which may open in response to glutamate-induced depolarisation. To determine the involvement of the latter pathway, blockade of $VGCa^{2+}$ channels was achieved either by application of nifedipine (100μM) or Cd^{2+} (50 μM). Co-application of glutamate and nifedipine partially reduced the amplitude of the $[Ca^{2+}]_i$ response (n=2, Fig. 12B). Similarly to nifedipine, Cd^{2+} block of $VGCa^{2+}$ channels in cells stimulated by glutamate resulted in a decreased in amplitude (n= 6), Fig. 12C). Interestingly, when $VGCa^{2+}$ channels were blocked before glutamate stimulation, the transient peak component of response was not apparent (Fig. 12B-C). These results indicate that $VGCa^{2+}$ channels, in part, mediate glutamate-elicited $[Ca^{2+}]_i$ increases in isolated HCs. Given the persistent rise in $[Ca^{2+}]_i$ during blockade of Ca^{2+} channels under glutamate application, and the complete elimination of Ca^{2+} glutamate response upon removal of Ca^{2+}_e, these data also suggest the involvement of glutamate receptors in Ca^{2+} influx.

3.7 Glutamate-elicited $[Ca^{2+}]_i$ Peak Amplitude is Decreased Under OGD Conditions

Excessive glutamatergic stimulation can be toxic to retinal neurons (Villani *et al.*, 1995; Ishikawa, 2013) unless adaptive mechanisms are able to blunt the deleterious effects of glutamate.

Figure 12. Glutamate-elicited (100 µM) increases in $[Ca^{2+}]_i$ depend upon extracellular Ca^{2+}. **(A)** Perfusion of 0 Ca^{2+} ECS during glutamate application eliminated increases in $[Ca^{2+}]_i$ (n=6). **(B)** 100 µM glutamate application during administration of 100 µM nifedipine reversibly increased resting $[Ca^{2+}]_i$ levels (n=2). **(C)** 100 µM glutamate application reversibly increased resting $[Ca^{2+}]_i$ levels during administration of 50 µM Cd^{2+} (n=6). Values presented are arbitrary fluorescent units of the fura-2 emission ratio 340 nm/380 nm. An increase in the ratio represents an increase in $[Ca^{2+}]_i$.

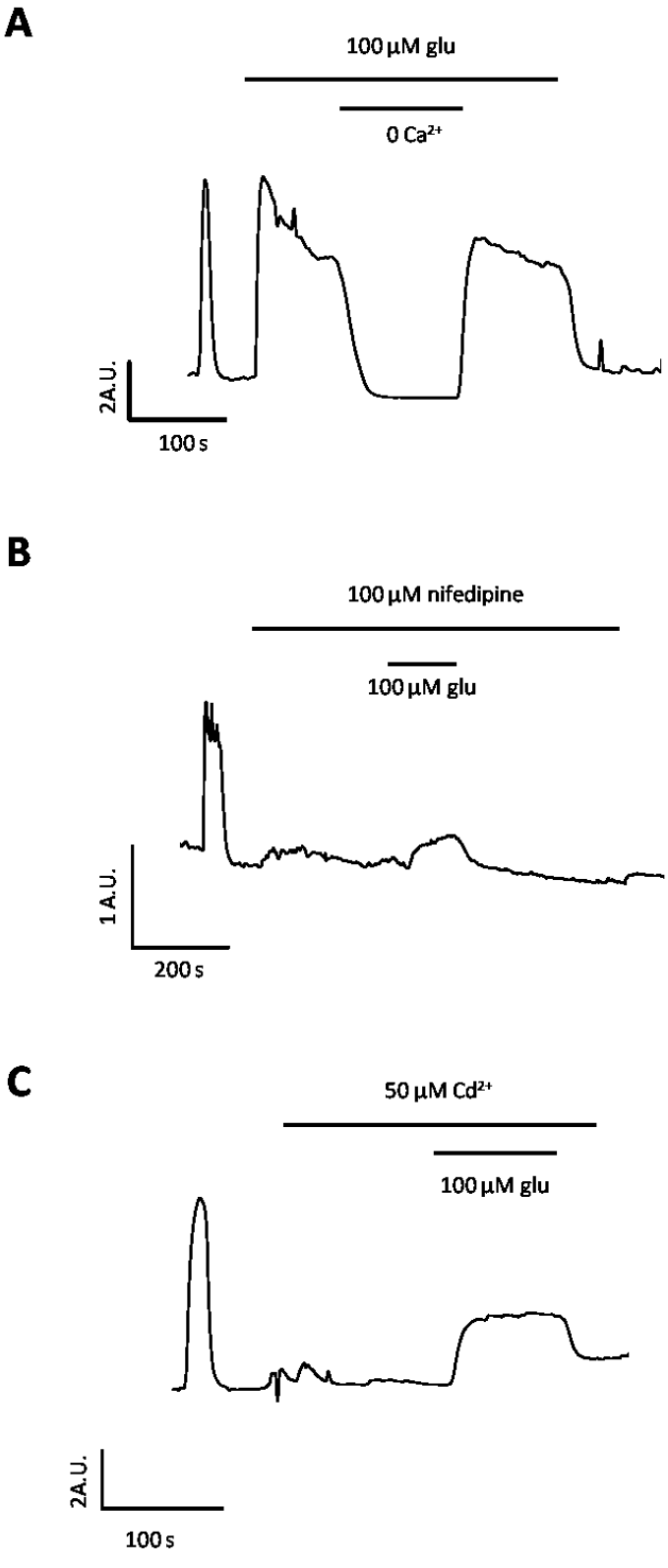
A
100 µM glu
0 Ca2+
2A.U.
100 s
B
100 µM nifedipine
100 µM glu
1A.U.
200 s
C
50 µM Cd2+
100 µM glu
2A.U.
100 s

To see if goldfish HCs show a reduction in glutamate-driven $[Ca^{2+}]_i$ responses under OGD, the peak and steady state amplitudes of glutamate-elicited events were measured, before OGD application, after 20 min of OGD, and after the cell had 5 min in normal perfusate. Similar to with spontaneous events, peak glutamate responses decreased in amplitude following OGD treatment (Fig. 13A). This decrease was significant between control, and OGD conditions, but did not recover following removal of the OGD (Fig. 13B, Friedman's test, n=6, with Dunn's comparison to control, $p<0.05$). Fluorescence decreased from a control value of 1 A.U. to 0.60 A.U. for both OGD and post-application conditions. There was no accompanying significant change in event steady state amplitude (Fig. 13C, Friedman's test, n=6, $P>0.05$, statistical summary in Suppl. Table IX). Sham experiments under in which cells were superfused with normal ECS over identical periods of time found no difference in peak or steady state amplitude glutamate responses (Wilcoxon, $P>0.05$, n=3, Suppl. Fig. 2, statistical summary in Supp. Table VIII). These data indicate that similarly to the amplitude of spontaneous Ca^{2+} events, the amplitude of the peak component of glutamate-elicited responses is also decreased under OGD conditions.

Figure 13. Effects of acute OGD treatment on glutamate (100 µM) – elicited $[Ca^{2+}]_i$ responses in isolated HCs. (A) Representative trace shows typical response of HCs to transient glutamate application before OGD, after 20 min in OGD, and after 5 min of normoxic perfusion (post-application condition). Values presented are arbitrary fluorescent units of the Fura-2 emission ratio 340 nm/380 nm, an increase in the ratio represents an increase in $[Ca^{2+}]_i$. **(B)** Comparison of peak glutamate response before and after 20 min of OGD, and after 5 min of normoxic recovery, both OGD and recovery groups were significantly different than the control (red asterisks) using Friedman's $p<0.05$, Dunn's post-hoc comparison to control, n=6 cells. **(C)** Comparison of steady state glutamate response amplitude before and after 20 min of OGD perfusion and after 5 min of recovery, there was no significant difference between groups. Friedman's $p>0.05$, n=6. Panels B-C: statistical summary can be found in Suppl. Tables IX.

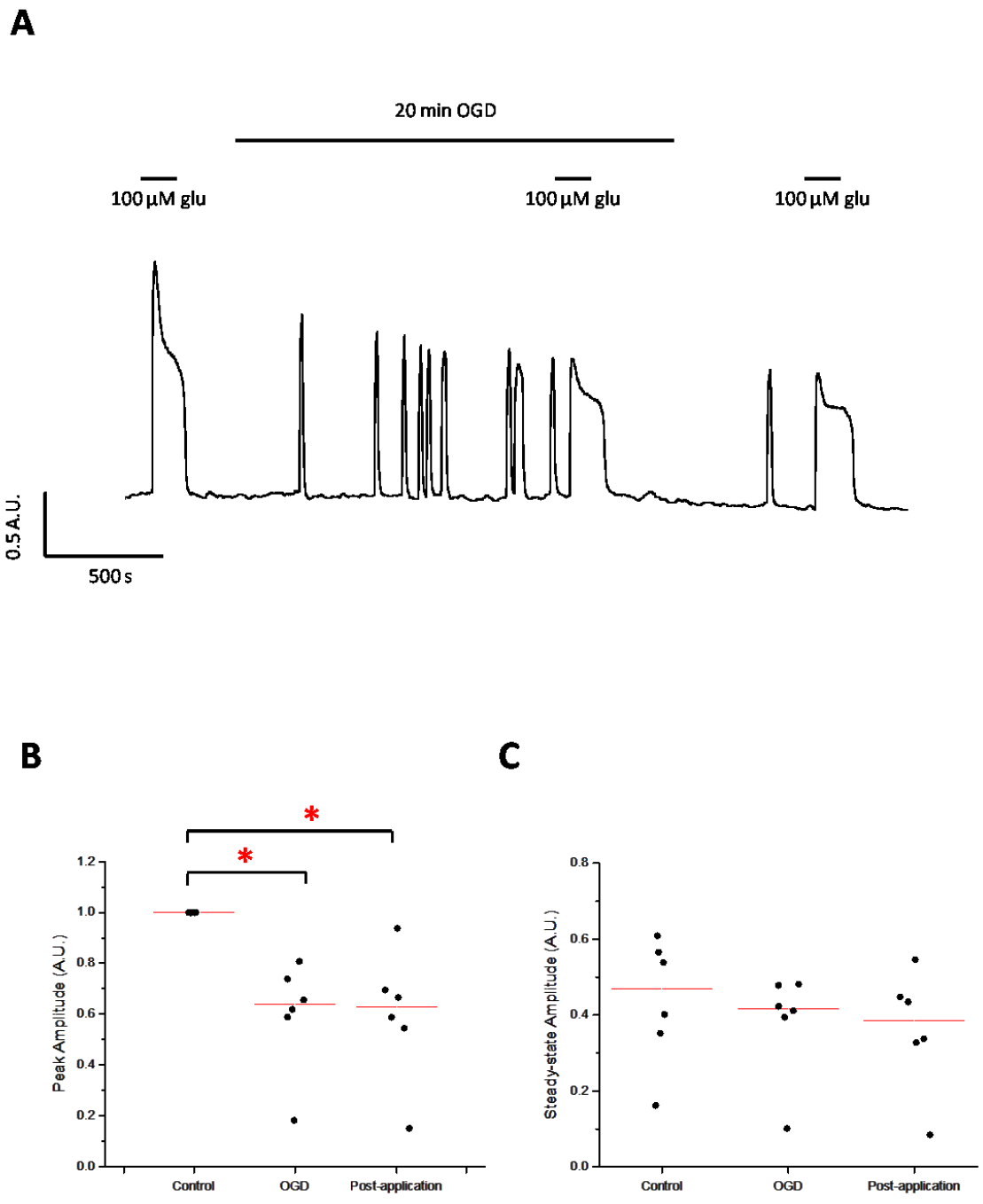
A
20 min OGD
100 µM glu
100 µM glu
100 µM glu
0.5 A.U.
500 s
B
C
*
*
Peak Amplitude (A.U.)
Steady-state Amplitude (A.U.)
Control
OGD
Post-application

4. Discussion

The initial characterisation of resting $[Ca^{2+}]_i$ dynamics of isolated HCs showed two stable baselines, between which HCs alternate. When the cell was in a lower baseline state, re-occurring, transient increases in $[Ca^{2+}]_i$ (spontaneous activity, SA) were observed. These transients were decreased in amplitude and AUC after acute insult with OGD. Under these conditions, the baseline $[Ca^{2+}]_i$ values did not change. This was unlike treatment with 0 glucose where an increase in baseline $[Ca^{2+}]_i$ was seen, indicating a potential protective effect of hypoxia. Similar OGD-mediated reductions were seen in the peak glutamate-elicited responses. This discussion will focus on the mechanisms that might regulate both spontaneous and glutamate-elicited $[Ca^{2+}]_i$ increases, and how these might change under conditions of low energy availability. Results from this thesis will be discussed within the context of retinal function and putative mechanisms for hypoxia tolerance.

4.1 Spontaneous and Resting $[Ca^{2+}]_i$ Dynamics of Isolated HCs

Spontaneous $[Ca^{2+}]_i$ activity (SA) of isolated teleost HCs has not been previously characterised in literature, though spontaneous AP generation has (Tachibana, 1981; Murakami & Takahashi, 1987; Dixon *et al.*, 1993; McMahon & Mattson, 1996; Cheng *et al.*, 2009). Spontaneous APs in goldfish HCs involve the opening of $VGCa^{2+}$ channels which conduct Ca^{2+} into the cell, depolarising the cell further, and elevating $[Ca^{2+}]_i$. The inward Ca^{2+} current is eventually inactivated by accumulation of $[Ca^{2+}]_i$, and voltage-inactivation of $VGCa^{2+}$ channels due to the antagonistic effects of transient and sustained outward K^+ currents (Tachibana, 1981, 1983). In the present work, SA was eliminated by blockade of $VGCa^{2+}$ channels with 50 μM Cd^{2+}, 100 μM nifedipine, or by removal of Ca^{2+}. Therefore, the waveform of spontaneous $[Ca^{2+}]_i$

transients observed in my preparation may be proportional to spontaneous AP amplitude and duration.

The bi-stability of HC V_m may explain the observed spontaneous changes in resting $[Ca^{2+}]_i$ baseline. The current-voltage properties of goldfish HCs are non-linear, and *in vivo* have two stable values of resting V_m: a hyperpolarised "bright light" V_m (~ -60 mV), and a more depolarised "dark" V_m (~ -30 mV) (Byzov & Trifonov YuA, 1981). At hyperpolarised potentials, $VGCa^{2+}$ are inactive; but at depolarised potentials, $VGCa^{2+}$ are constitutively active, which would increase $[Ca^{2+}]_i$ to a higher level; maintained steady by increased Ca^{2+} exchange current and activity of membrane pumps (Hayashida *et al.*, 1998). Glutamate application during periods of elevated $[Ca^{2+}]_i$ baseline or during very long (min) spontaneous events caused further increases in $[Ca^{2+}]_i$, but returned the baseline to a lower steady state upon washout. This could be explained by the increased Ca^{2+} influx causing subsequent inactivation of $VGCa^{2+}$ channels, which upon removal of glutamate may allow outward K^+ currents to lower the V_m, and Ca^{2+} extrusion mechanisms to catch up (Hayashida & Yagi, 2002*a*). It would be interesting if the spontaneous changes in resting baseline could be explained by V_m bi-stability, but this will require concurrent electrophysiological recording of V_m.

SA was eliminated by removal of Ca^{2+}_e, and this was followed by a large and sustained $[Ca^{2+}]_i$ increase (lasting minutes) upon return of Ca^{2+}_e to the recording solution. Goldfish HCs have hemichannels that would depolarise the cell when opened (Kamermans *et al.*, 2001), and hemichannel activation occurs under conditions of low $[Ca^{2+}]_e$ (Jonz & Barnes, 2007). Thus opening of hemichannels may have brought V_m to a more depolarised state, at which activated $VGCa^{2+}$ currents increased $[Ca^{2+}]_i$ during reperfusion with normal solution. Alternatively, store-operated Ca^{2+} channels (SOC) on goldfish HCs have been implicated in triggering $[Ca^{2+}]_i$

increases upon removal and replacement of $[Ca^{2+}]_e$ (Lv *et al.*, 2014). Either of these mechanisms could explain the sustained increase in $[Ca^{2+}]_i$ observed upon reperfusion with Ca^{2+}_e, though blocking experiments are required to confirm either. It is interesting to note that Lv. *et al*. (2014) used 2-APB to demonstrate the presence of SOCs in goldfish HCs. 2-APB is also known to be a direct inhibitor of Cx26 (Tao & Harris, 2007), which is the main Cx component of fish HC gap junctions and hemichannels (Kamermans *et al.*, 2001; Twig *et al.*, 2003).

SA was observed in all cells examined, though the frequency and waveform of SA events differed between cells. The literature describing variation of spontaneous APs is lacking. The only hint comes from Tachibana, who mentioned that fluctuations in resting V_m were large enough to elicit APs in roughly 50% of cells examined (Tachibana, 1981). He also noted that the duration of elicited APs lasted between 2 and 6 s, although others have noted spontaneous APs lasting several minutes (Shingai & Christensen, 1986; Murakami & Takahashi, 1987). The majority of the events we observed lasted between 8 and 40 s, which are longer than the durations of APs reported by Tachibana. This discrepancy in duration may indicate differences in cell preparation, that spontaneous $[Ca^{2+}]_i$ events are generated through different mechanisms, or are shaped additionally by Ca^{2+} extrusion, sequestration, and release from intracellular stores. Indeed, non-AP-related caffeine-induced $[Ca^{2+}]$ oscillations in goldfish HCs have been described, generated by RyR activation, release of sarcoplasmic Ca^{2+}, and dissipation by sarcoplasmic and membrane pumps and exchangers (Lv *et al.*, 2014). These oscillations are limited by the duration and concentration of caffeine application, and were still present during application of nifedipine or removal of $[Ca^{2+}]_e$ (*ibid,* 2014). As such they likely do not represent

the same phenomenon described in this thesis, but that does not exclude the contribution of alternative mechanisms of Ca^{2+} entry facilitating SA.

Only one paper has discussed similar regular, spontaneous $[Ca^{2+}]_i$ events. While monitoring H^+ fluxes close to the membranes of isolated goldfish HCs, Kreitzer *et al*. noted 3 phenotypes of H^+ signals: standing positive signals (H^+_e increase), standing negative signals (H^+_e decrease), and also spontaneous oscillations in H^+_e (Kreitzer *et al.*, 2012). Both nifedipine and $[Ca^{2+}]_e$ removal eliminated spontaneous oscillations in H^+, and oscillations in H^+ were shown to overlap with oscillations in microspectrofluorometric measurements of $[Ca^{2+}]_i$ (though characterisation of spontaneous $[Ca^{2+}]_i$ changes and investigation of $[Ca^{2+}]_i$ baselines were not explored). These experiments in part led the authors to conclude that the oscillations in H^+ were due to changes in $[Ca^{2+}]_i$ which activated Ca^{2+} pumps that exchange Ca^{2+}_i for H^+_e (Kreitzer *et al.*, 2012). The bi-stability and oscillatory nature of the H^+ signal shown by Kreitzer *et al.* (2012) likely then corroborates that of $[Ca^{2+}]_i$ shown in this thesis; unfortunately these authors did not any provide further characterisation or explanation.

Unlike with SA, the $[Ca^{2+}]_i$ response to glutamate has been characterised in HCs. In the present study, 100 μM glutamate provoked a transient peak and then a sustained increase in $[Ca^{2+}]_i$. This response matches those described in fish HCs for glutamate (Hayashida *et al.*, 1998) and AMPA application (Huang *et al.*, 2004). The AMPA-triggered transient $[Ca^{2+}]_i$ peak was demonstrated in goldfish HCs to be partially dependent on CICR (Huang *et al.*, 2004). This was also shown for glutamate-elicited peaks in carp HCs (Hayashida & Yagi, 2002*a*). In the present work, pre-incubation of HCs in 100 μM nifedipine or 50 μM Cd^{2+} eliminated the transient peak. If this transient peak is generated mostly as a result of CICR, then the lack of peak under $VGCa^{2+}$ channel blockade may indicate that Ca^{2+} influx through iGlurRs is not sufficient to

trigger CICR (Solessio & Lasater, 2002). In the present experiments, only removal of $[Ca^{2+}]_e$ eliminated the steady state $[Ca^{2+}]_i$ response to glutamate, while application of 100 μM nifedipine or 50 μM Cd^{2+} reduced the response, but did not eliminate it, implying that both Ca^{2+} influx through iGlurR and $VGCa^{2+}$ channels are involved. This matches data from carp HCs, which demonstrate additionally that the Ca^{2+} influx through both glutamate and $VGCa^{2+}$ channels is counter-balanced by the activities of the membrane Na^+/Ca^+ exchanger, and the Ca^{2+}ATPase (Hayashida *et al.*, 1998; Hayashida & Yagi, 2002*a*).

4.2 Spontaneous and Elicited Ca^{2+} Activity - Effect of OGD

Both amplitude and AUC of SA activity decreased significantly within 20 min of OGD or glucose removal. There were no large changes in the duration of SA between treatments, and so the reduction in AUC was likely due to lowered SA amplitude. The magnitude of the decrease varied between cells, which may indicate differential cell viability, or intrinsic differences in Ca^{2+} dynamics of HC subtypes. For example, light responses of goldfish rod HCs were shown to be more sensitive to $[Ca^{2+}]_e$ modulation *in vivo* than those of cone HCs (Rowe, 1987).

Without identifying the mechanisms that govern SA, it is difficult to meaningfully speculate on the pathways facilitating their reduction. If SA is dictated mostly by spontaneous APs, up-regulated outward K^+ currents would reduce the amplitude of $VGCa^{2+}$ currents (Tachibana, 1981) and therefore blunt increases in SA. Increased K^+ efflux is seen in mammalian neurons during the initial phase of ischemic challenge, and this is thought to reduce immediate excitotoxicity under low energy conditions, but is actually less efficient at maintaining V_m in the long term (Bickler & Buck, 1998). A reduction in Ca^{2+} currents would be neuroprotective, as it both decreases $[Ca^{2+}]_i$ and weakens the depolarisation of HCs. Direct demonstration of hypoxic

$VGCa^{2+}$ arrest is lacking, but it has been implicated as protective in neurons of hypoxia-tolerant organisms (Bickler, 1992; Staples & Buck, 2009). Decreased activity of $VGCa^{2+}$ channels could be mediated by intracellular signalling pathways. For example, suppression of $VGCa^{2+}$ currents though activation of calmodulin and CaMKII has been demonstrated in catfish HCs (Linn & Gafka, 2001). Intracellular acidification is also known to reduce Ca^{2+} currents in isolated HCs (Dixon *et al.*, 1993). Even if V_m-related components of SA remain constant, a reduction in transient $[Ca^{2+}]_i$ amplitude could be achieved by up-regulated Ca^{2+} extrusion mechanisms, though this would require increased ATP use to maintain ionic homeostasis and would therefore not be adaptive (Buck & Bickler, 1998).

A reduction in the magnitude of CICR in HCs could also explain SA suppression, especially given a similar decrease was seen in the peak (but not steady state) glutamate response, which is likely shaped by CICR (Huang *et al.*, 2004). CICR has been implicated in mediating toxic increases in $[Ca^{2+}]_i$ in retinal ischemia (Osborne *et al.*, 2004), which could be problematic to teleost HCs known for CICR resulting in 10- to 30-fold increases in $[Ca^{2+}]_i$ (Hayashida *et al.*, 1998; Solessio & Lasater, 2002; Huang *et al.*, 2004).

In addition to altered CICR, the reduction of the peak glutamate response may be affected by altered activity of glutamate receptors. Up-regulation of Ca^{2+}-permeable AMPA-Rs contributing to excitotoxicity is seen in mammalian stroke (Kwak & Weiss, 2006). Both Ca^{2+}-permeable and impermeable AMPA-Rs are expressed on goldfish HCs (Huang & Liang, 2005), and Ca^{2+}-permeable AMPA-Rs have been shown to contribute relatively more to the glutamate response of carp HCs (Sun *et al.*, 2010). Reducing the contribution of Ca^{2+}-permeable receptors would blunt Ca^{2+} influx. Alternatively, AMPA-Rs could be down regulated in a similar manner as in turtle brain involving mK_{ATP} activation and channel dephosphorylation (Pamenter *et al.*,

2008*a*), though this pathway has not been tested in goldfish. OGD mediated decreases in Ca^{2+} flux though $VGCa^{2+}$ or AMPA-Rs may be less important than CICR given the constancy of the steady-state component of the glutamate response which in carp is determined by Ca^{2+} influx through iGlurRs and $VGCa^{2+}$ channels, but further investigation is required.

Because SA was reduced after both OGD and 0 glucose treatments, mechanisms of their reduction may be similarly tied to decreased glucose levels or that both responses are processed through a convergent sensory pathway and effector system (e.g. mK_{ATP} channels or AMPK). For example, AMPK senses decreases in energy charge (an index of [ATP], [ADP], and [AMP], that informs cellular energy status) brought about by either low O_2 and/or low glucose (Renshaw & Nikinmaa, 2007).

The lack of SA and peak glutamate amplitude recovery following re-introduction of O_2 and glucose could be due to signalling cascades that do not reverse in a timely manner. This is seen for the decreased NMDA-elicited $[Ca^{2+}]_i$ transients in anoxic isolated turtle neurons (Bickler *et al.*, 2000) and hypoxic reduction in NMDA-R currents in goldfish brain (Wilkie *et al.*, 2008), which were demonstrated without recovery. This lack of recovery could be due to the time frames examined (10s of minutes), or be explained by damage sustained during or after the insult. For example ROS generation following re-oxygenation has been implicated in permanently lowering the activity of fish membrane Na^+/K^+ ATPases (Wilkie *et al.*, 2008).

The increase in $[Ca^{2+}]_i$ baseline during or following glucose removal under normoxic conditions did not recover (indicating a lack of homeostatic control). A decrease in SA amplitude was seen for both OGD and glucose removal but absolute $[Ca^{2+}]_i$ measurements were not made, so the possibility remains that $[Ca^{2+}]_i$ events were suppressed to a greater degree during OGD (acting through an O_2-dependent signalling pathway), affording those cells the ability to maintain

baseline $[Ca^{2+}]_i$ within manageable levels. Additionally, maintained baseline $[Ca^{2+}]_i$ may indicate a suppressed, sustained, or augmented permeability to Ca^{2+}, but would not appear different if coupled to extrusion or sequestration mechanisms that match influx. Reducing the turnover of $[Ca^{2+}]_i$ would be protective, and maintaining or increasing turnover could be damaging under energy stressed conditions (Buck & Hochachka, 1993; Staples & Buck, 2009). Studies from *Carassius* have shown that adaptive signalling pathways are differentially activated upon the severity of low energy stressor (Stensløkken *et al.*, 2008*b*). Therefore, it could be that protective signalling requires a more intense change in energy charge (Staples & Buck, 2009).

ROS can also act as signalling messengers in HCs (Zhou *et al.*, 2001). ROS production of HCs would be expected to be less (although not absent) under OGD as O_2 is required for its formation. ROS production (or other O_2-dependent signalling) under OGD and 0 glucose conditions could have input upon pathways that facilitate suppressed SA, or on resting membrane ion homeostasis.

4.3 Limitations of the Model and Implications Hypoxia Tolerance

Taken alone, a reduction in SA and the protective effect of O_2 removal on maintaining baseline $[Ca^{2+}]_i$ supports the premise that goldfish HCs show adaptive responses to some conditions of restricted energy availability. However, a clear elucidation of the mechanisms governing SA generation and suppression is required to substantiate this claim. *In vivo* though, goldfish HCs are not necessarily afforded chemical and electrical isolation during hypoxia. It is challenging to explain roles that suppression of $[Ca^{2+}]_i$ activity in isolated HCs may have upon the retina as a whole, given the limitations of the model and paucity of literature on the subject.

The isolated neuron model used requires the cell's removal from all normal synaptic input and extracellular environment. HCs make many synaptic contacts, including dopaminergic input from IPL cells, glutamatergic input from PRs, gap junctions with other HCs (Kolb *et al.*, 2001) as well as possibly important autocrine GABA signalling (Paik *et al.*, 2003; Liu *et al.*, 2013). This removal can change the responses of cells. For example only isolated HCs have been shown to display spontaneous APs (Murakami & Takahashi, 1987); though APs can be generated *in situ* under conditions that potentiate Ca^{2+} currents and repress K^{+} currents (Murakami & Takahashi, 1988). Luckily, basic HC current-voltage relationships remain conserved in isolated cells (Byzov & Trifonov YuA, 1981; Tachibana, 1983), as well as HCs' responses to neurotransmitters; for example glutamate (Tachibana, 1985) or dopamine (McMahon & Mattson, 1996).

Mammalian retinal ischemia is well studied (Osborne *et al.*, 2004), but this is not the case in fish (Kato *et al.*, 1997*b*), and it is unknown if the goldfish retina actually experiences ischemia. During hypoxia, brain blood flow and cardiac output remain stable in *Carassius* (Nilsson & Lutz, 2004; Stensløkken *et al.*, 2014), and circulating blood glucose actually increases (Walker & Johansen, 1977; Lutz & Nilsson, 1997). The teleost retina though is avascular and quite thick (Kato *et al.*, 1991; Waser & Heisler, 2005) and local measurements of blood flow of the choroid rete supplying the retina, or transfer of energetic substrates, have not been carried out under hypoxia or ischemia. In addition, electrical activity in both the visual (Johansson *et al.*, 1997) and auditory systems (Fay & Ream, 1992) of *Carassius* are very suppressed under anoxia, whereas whole brain electrical activity remains more constant in these fish (Nilsson & Lutz, 2004). Therefore the possibility remains that metabolic supply to specific areas of the CNS is reduced. Regardless, use of an OGD model is still interesting as both hypoxic and ischemic damage are rooted in limited energy availability during these insults, and

tolerance mechanisms to both are expected to be similar (Bickler, 2004; Pamenter *et al.*, 2012; Galli & Richards, 2014).

The suppression (up to 90%) of retinal electrical activity in anoxic *Carassius* was demonstrated (Johansson *et al.*, 1997), but how this is mediated is unknown. Proposed mechanisms include GABA-ergic suppression, as well as ion channel arrest as both are known to be inhibitory in *Carassius* brain during conditions of low O_2 (Stensløkken *et al.*, 2008*a*; Wilkie *et al.*, 2008). Interestingly, in several hypoxia-tolerant species, the b-wave of the ERG (thought to reflect signal transmission from PRs to GCs) is affected more than the a-wave (PR responses), which may imply that electrical inhibition in the retina occurs more importantly at the signal processing level between retinal neurons (Stensløkken *et al.*, 2008*a*). HCs could play a complex role in this suppression, given that they themselves would need to adapt to survive energy deprivation, but could also provide an inhibitory element as they are set up to provide inhibitory feedback under normal circumstances.

Spontaneous APs are thought to be a manifestation of the efficient transition between hyperpolarised and depolarised potentials under different illumination conditions (Byzov & Trifonov YuA, 1981; Tachibana, 1981). If OGD-mediated SA suppression is related to a reduction of AP amplitude, this may provide for a reduced load on HC ionic homeostatic regulation which would be protective, but could also have implications for HC-mediated feedback which is dependent on V_m. From a Ca^{2+}-centric perspective, a reduction in SA could impact Ca^{2+}-mediated feedback of HCs (Huang *et al.*, 2006; Jackman *et al.*, 2011), modulation of synapse formation (Okada *et al.*, 1999), or gating of gap junctions and hemichannels (McMahon & Mattson, 1996). Whether each of these Ca^{2+} related functions would lead to more or less inhibitory feedback is uncertain given that universal mechanisms of HC feedback have

not been established and may vary depending upon HC subtype or situation (Thoreson & Mangel, 2012). Increases in $[Ca^{2+}]_i$ have been linked to HC spinule retraction which reduces glutamatergic input from PRs to HCs (Okada *et al.*, 1999). Although reduced glutamate would be protective for HCs, synaptic contacts are required for HC negative feedback onto PRs, and so a reduction in $[Ca^{2+}]_i$ could prolong the amount of time that HCs can mediate inhibitory feedback for. Of course there are many other factors that regulate HC spinule formation including light, dopamine, nitric oxide, et cetera, and the balance of whether spinules will remain intact will depend on the synergistic outcome of whole retina function. This speculatory example demonstrates that mapping out the *in vivo* responses of HCs, and how HC $[Ca^{2+}]_i$ changes interplay with the many cell types they are synapsed with will help in determining how observed retinal electrical depression is accomplished.

It has been suggested that a more general role for HCs in mediating retinal electrical depression could lie in providing GABA-ergic tone (Johansson *et al.*, 1997) as is seen in the hypoxia-tolerant brain (Buck *et al.*, 2012). Goldfish H1 can synthesise, and release GABA, although other HC types cannot (Paik *et al.*, 2003). The uptake of GABA is thought to be mostly mediated by HCs and is V_m dependent, increasing with hyperpolarisation, and reverses upon depolarisation, facilitating GABA release (Lam & Ayoub, 1983). Accumulation of $[Ca^{2+}]_i$ causes reduced GABA uptake in HCs (Kreitzer *et al.*, 2003), and reduced uptake of synaptic GABA has been implicated in partially mediating GABA-ergic suppression in the *Carassius* brain (Ellefsen *et al.*, 2008). If OGD suppresses $[Ca^{2+}]_i$, it could lead to altered GABA uptake (depending on the depolarisation state of the cell). How this translates to retinal suppression is complicated since in goldfish, cones and BPs possess GABA-gated currents, but these can be either excitatory or inhibitory. For example, cones possess $GABA_A$ receptors that cause them to hyperpolarise upon

GABA application, but BCs possess $GABA_A$ receptors which hyperpolarise or depolarise them depending on the transmembrane chloride gradient of the cell in question (Twig *et al.*, 2003). Therefore if HC-mediated GABA inhibition is important, it is likely not the global electrical depressant that it is in the brain.

The potentially protective OGD suppression of $[Ca^{2+}]_i$ of goldfish HCs may just serve to protect that specific retinal cell type, with other retinal cell types displaying similar decreases. Alternatively, other cell types may play more prominent roles in whole retinal depression. In the goldfish retina, PRs release and re-uptake glutamate from the synaptic cleft, with MCs providing important glutamate clearance function (Vandenbranden & Verweij, 1996). Decreased glutamate release from PRs onto BCs and HCs, as well as increased uptake of glutamate into PRs and MCs would limit whole retina excitability (though this would also require controlled ionic homeostasis). Increased glutamate uptake and blocking release is known to be neuro-protective in the retina (Ishikawa, 2013), but adaptive examples of this remains to be identified in the retina of hypoxia-tolerant species. Even if HCs do not mediate whole retinal suppression, they may still usefully serve as a model CNS neurons of tolerance.

4.4 Summary and Perspectives

The demonstration of this thesis that isolated HCs of the goldfish retina display spontaneous transient increases in $[Ca^{2+}]_i$ and changes in stable baseline levels is interesting given the multitude of roles which this ion has been implicated in, contributing to both synaptic plasticity and signal processing in the retina (Lv *et al.*, 2014). The genesis of these transients was shown to require entry of Ca^{2+} from extracellular sources, but their proximal cause (whether AP-

related or not), and regulation under conditions of limited energy availability remains to be determined.

OGD and glucose removal were shown to decrease the amplitude and AUC of transients, which was similarly seen in the OGD-mediated reduction of the peak glutamate response. While the reductions seen may relate to adaptive cellular responses, determination of the mechanisms of SA generation and regulation are required for further understanding their significance. These contenders include: V_m changes, flux of Ca^{2+} through voltage- or receptor-gated channels, ATP-powered extrusion, buffering, and the activity of intracellular stores. The relative contributions of all these mechanisms can be separated using pharmacological isolation of components, coupled to simultaneous monitoring of V_m and $[Ca^{2+}]_i$ (Hayashida & Yagi, 2002*b*). Monitoring pH_i and ROS production in addition to Ca^{2+} will contribute to a more holistic picture of changing cellular physiology allowing for more targeted determination of possible signalling pathways. By calibrating Fura-2 measurements to standards, determination of absolute variation in $[Ca^{2+}]_i$ is possible (Grienberger & Konnerth, 2012), which will be informative in linking changes in $[Ca^{2+}]_i$ dynamics to protective or toxic levels. This is especially important given the effect of hypoxia on maintenance of baseline $[Ca^{2+}]_i$ stability during glucose removal. Low sample sizes have limited the ability to discriminate between possible different patterns of SA, and effects of energetic stress which may be specific to HC subtypes (Kreitzer *et al.*, 2012). In addition, mapping out the *in vivo* responses of HCs, and how HC $[Ca^{2+}]_i$ changes interplay with the many cell types they are synapsed with will help determine how observed retinal electrical depression is accomplished, and whether HC function is even important in mediating this phenomenon. Fish retinal slice preparations have been developed allowing for integrative monitoring of cell responses within a neural network (Vessey *et al.*, 2005).

The work presented in this thesis gives an intriguing hint towards demonstrating cellular adaptive responses to conditions of low energy availability. No one single process is responsible for the exquisite resilience of the goldfish, or any hypoxia-tolerant animal. Identifying the contributions and interactions of changes at the cellular, tissue, organismal, and environmental level will allow for a better understanding of how these vertebrates have evolved to tolerate conditions that mammals, including humans, cannot survive. Perhaps such research directions may offer clues as to how hypoxia-intolerant species may better survive under low O_2.

References

Ankarcrona M, Dypbukt JM, Bonfoco E, Zhivotovsky B, Orrenius S, Lipton SA & Nicotera P (1995). Glutamate-induced neuronal death: a succession of necrosis or apoptosis depending on mitochondrial function. *Neuron* **15,** 961–973.

Bickler PE (1992). Cerebral anoxia tolerance in turtles: regulation of intracellular calcium and pH. *Am J Physiol* **263,** R1298–R1302.

Bickler PE (2004). Clinical perspectives: neuroprotection lessons from hypoxia-tolerant organisms. *J Exp Biol* **207,** 3243–3249.

Bickler PE & Buck LT (1998). Adaptations of vertebrate neurons to hypoxia and anoxia: maintaining critical Ca^{2+} concentrations. *J Exp Biol* **201,** 1141–1152.

Bickler PE & Buck LT (2007). Hypoxia tolerance in reptiles, amphibians, and fishes: life with variable oxygen availability. *Annu Rev Physiol* **69,** 145–170.

Bickler PE, Donohoe PH & Buck LT (2000). Hypoxia-induced silencing of NMDA receptors in turtle neurons. *J Neurosci* **20,** 3522–3528.

Boutilier RG (2001). Mechanisms of cell survival in hypoxia and hypothermia. *J Exp Biol* **204,** 3171–3181.

Buck LT & Bickler PE (1998). Adenosine and anoxia reduce N-methyl-D-aspartate receptor open probability in turtle cerebrocortex. *J Exp Biol* **201,** 289–297.

Buck LT & Hochachka PW (1993). Anoxic suppression of Na(+)-K(+)-ATPase and constant membrane potential in hepatocytes: support for channel arrest. *Am J Physiol* **265,** R1020–R1025.

Buck LT, Hogg DWR, Rodgers-Garlick C & Pamenter ME (2012). Oxygen sensitive synaptic neurotransmission in anoxia-tolerant turtle cerebrocortex. ed. Nurse CA, Gonzalez C, Peers C & Prabhakar N. *Adv Exp Med Biol* **758,** 71–79.

Byzov AL & Trifonov JA (1968). The response to electric stimulation of horizontal cells in the carp retina. *Vision Res* **8,** 817–822.

Byzov AL & Trifonov YuA (1981). Ionic mechanisms underlying the nonlinearity of horizontal cell membrane. *Vision Res* **21,** 1573–1578.

Cheng N, Tsunenari T & Yau K-W (2009). Intrinsic light response of retinal horizontal cells of teleosts. *Nature* **460,** 899–903.

Choi DW (1992). Excitotoxic cell death. *J Neurobiol* **23,** 1261–1276.

Contreras JE, Sánchez H a, Véliz LP, Bukauskas FF, Bennett MVL & Sáez JC (2004). Role of connexin-based gap junction channels and hemichannels in ischemia-induced cell death in nervous tissue. *Brain Res Brain Res Rev* **47,** 290–303.

Crawshaw LI, Wollmuth LP & O'Connor CS (1989). Intracranial ethanol and ambient anoxia elicit selection of cooler water by goldfish. *Am J Physiol* **256,** R133–R137.

Dixon DB, Takahashi K, Bieda M & Copenhagen DR (1996). Quinine, intracellular pH and modulation of hemi-gap junctions in catfish horizontal cells. *Vision Res* **36,** 3925–3931.

Dixon DB, Takahashi K & Copenhagen DR (1993). L-glutamate suppresses HVA calcium current in catfish horizontal cells by raising intracellular proton concentration. *Neuron* **11,** 267–277.

Djamgoz MB & Stell WK (1984). Tetrodotoxin does not block the axonal transmission of S-potentials in goldfish retina. *Neurosci Lett* **49,** 233–238.

Dorigatti M, Krumschnabel G, Schwarzbaum PJ & Wieser W (1997). Effects of Hypoxia on Energy Metabolism in Goldfish Hepatocytes. *Comp Biochem Physiol Part B Biochem Mol Biol* **117,** 151–158.

Dvoriantchikova G, Ivanov D, Barakat D, Grinberg A, Wen R, Slepak VZ & Shestopalov VI (2012). Genetic ablation of Pannexin1 protects retinal neurons from ischemic injury. *PLoS One* **7,** e31991.

Ellefsen S, Stenslokken K-O, Fagernes CE, Kristensen T, & Nilsson GE (2008). Expression of genes involved in GABAergic neurotransmission in anoxic crucian carp brain (*Carassius carassius*). *Physiol Genomics* **36,** 61–68.

Euler T, Haverkamp S, Schubert T & Baden T (2014). Retinal bipolar cells: elementary building blocks of vision. *Nat Rev Neurosci* **15,** 507–519.

Fago A & Jensen FB (2015). Hypoxia tolerance, nitric oxide, and nitrite: lessons from extreme animals. *Physiology (Bethesda)* **30,** 116–126.

Fahrenfort I, Klooster J, Sjoerdsma T & Kamermans M (2005). The involvement of glutamate-gated channels in negative feedback from horizontal cells to cones. *Prog Brain Res* **147,** 219–229.

Fahrenfort I, Steijaert M, Sjoerdsma T, Vickers E, Ripps H, van Asselt J, Endeman D, Klooster J, Numan R, ten Eikelder H, von Gersdorff H & Kamermans M (2009). Hemichannel-mediated and pH-based feedback from horizontal cells to cones in the vertebrate retina. *PLoS One* **4,** e6090.

Fay RR & Ream TJ (1992). The effects of temperature change and transient hypoxia on auditory nerve fiber response in the goldfish (*Carassius auratus*). *Hear Res* **58,** 9–18.

Gallego A (1986). Chapter 7 Comparative studies on horizontal cells and a note on microglial cells. *Prog Retin Res* **5,** 165–206.

Galli GLJ & Richards JG (2014). Mitochondria from anoxia-tolerant animals reveal common strategies to survive without oxygen. *J Comp Physiol B* **184,** 285–302.

Grienberger C & Konnerth A (2012). Imaging calcium in neurons. *Neuron* **73,** 862–885.

Grynkiewicz G, Poenie M & Tsien RY (1985). A new generation of Ca^{2+} indicators with greatly improved fluorescence properties. *J Biol Chem* **260,** 3440–3450.

Hankins MW & Ikeda H (1993). Consequences of transient retinal hypoxia on rod input to horizontal cells in the rat retina. *Vision Res* **33,** 429–436.

Hayashida Y & Yagi T (2002*a*). On the interaction between voltage-gated conductances and Ca(2+) regulation mechanisms in retinal horizontal cells. *J Neurophysiol* **87,** 172–182.

Hayashida Y & Yagi T (2002*b*). Contribution of Ca^{2+} transporters to electrical response of a non-spiking retinal neuron. *Neurocomputing* **44-46,** 7–12.

Hayashida Y, Yagi T & Yasui S (1998). Ca^{2+} regulation by the Na(+)-Ca(2+) exchanger in retinal horizontal cells depolarized by L-glutamate. *Neurosci Res* **31,** 189–199.

Hitchcock PF & Easter SS (1986). Retinal ganglion cells in goldfish: a qualitative classification into four morphological types, and a quantitative study of the development of one of them. *J Neurosci* **6,** 1037–1050.

Hochachka PW (1986). Defense strategies against hypoxia and hypothermia. *Science* **231,** 234–241.

Hochachka PW, Buck LT, Doll CJ & Land SC (1996). Unifying theory of hypoxia tolerance: molecular/metabolic defense and rescue mechanisms for surviving oxygen lack. *Proc Natl Acad Sci U S A* **93,** 9493–9498.

Huang S-Y, Hu J-F, Gong H-Q & Liang P-J (2006). Postsynaptic calcium pathway contributes to synaptic plasticity between retinal cones and luminosity-type horizontal cells. *Sheng Li Xue Bao* **58,** 407–414.

Huang S-Y & Liang P (2005). Ca^{2+}-permeable and Ca^{2+}-impermeable AMPA receptors coexist on horizontal cells. *Neuroreport* **16,** 263–266.

Huang S-Y, Liu Y & Liang P-J (2004). Role of Ca^{2+} store in AMPA-triggered Ca^{2+} dynamics in retinal horizontal cells. *Neuroreport* **15,** 2311–2315.

Ishida AT, Kaneko A & Tachibana M (1984). Responses of solitary retinal horizontal cells from *Carassius auratus* to L-glutamate and related amino acids. *J Physiol* **348,** 255–270.

Ishida AT & Neyton J (1985). Quisqualate and L-glutamate inhibit retinal horizontal-cell responses to kainate. *Proc Natl Acad Sci U S A* **82,** 1837–1841.

Ishikawa M (2013). Abnormalities in glutamate metabolism and excitotoxicity in the retinal diseases. *Scientifica (Cairo)* **2013,** 528940.

Jackman S, Babai N & Chambers J (2011). A positive feedback synapse from retinal horizontal cells to cone photoreceptors. *PLoS Biol* **9,** e1001057.

Johansson D & Nilsson G (1995). Roles of energy status, K_{ATP} channels and channel arrest in fish brain K+ gradient dissipation during anoxia. *J Exp Biol* **198,** 2575–2580.

Johansson D, Nilsson GE & Døving KB (1997). Anoxic depression of light-evoked potentials in retina and optic tectum of crucian carp. *Neurosci Lett* **237,** 73–76.

Johnston D & Lam DM (1981). Regenerative and passive membrane properties of isolated horizontal cells from a teleost retina. *Nature* **292,** 451–454.

Jonz MG & Barnes S (2007). Proton modulation of ion channels in isolated horizontal cells of the goldfish retina. *J Physiol* **581,** 529–541.

Kamermans M, Fahrenfort I, Schultz K, Janssen-Bienhold U, Sjoerdsma T & Weiler R (2001). Hemichannel-mediated inhibition in the outer retina. *Science* **292,** 1178–1180.

Kaneko A (1970). Physiological and morphological identification of horizontal, bipolar and amacrine cells in goldfish retina. *J Physiol* **207,** 623–633.

Kato S, Negishi K, Teranishi T & Ishita S (1991). The use of the carp retina in neurobiology: its uniqueness and application for neural network analyses of the inner retina. *Prog Neurobiol* **37,** 287–327.

Kato S, Shou Z, Sugawara K, Yasui Y, N.Takizawa, Sugitani K & Mawatari K (1997*a*). Ischemic neuronal death in the fish retina in respect of oxygen redicals and glutathione. In *Degenerative Retinal Diseases* Springer US, Boston, MA.

Klooster J, Studholme KM & Yazulla S (2001). Localization of the AMPA subunit GluR2 in the outer plexiform layer of goldfish retina. *J Comp Neurol* **441,** 155–167.

Knapp a G, Schmidt KF & Dowling JE (1990). Dopamine modulates the kinetics of ion channels gated by excitatory amino acids in retinal horizontal cells. *Proc Natl Acad Sci U S A* **87,** 767–771.

Kolb H, Nelson R, Ahnelt P & Cuenca N (2001). Cellular organization of the vertebrate retina. *Prog Brain Res* **131,** 3–26.

Kramer DL (1987). Dissolved oxygen and fish behavior. *Environ Biol Fishes* **18,** 81–92.

Kreitzer M a, Andersen K a & Malchow RP (2003). Glutamate modulation of GABA transport in retinal horizontal cells of the skate. *J Physiol* **546,** 717–731.

Kreitzer M a, Jacoby J, Naylor E, Baker A, Grable T, Tran E, Booth SE, Qian H & Malchow RP (2012). Distinctive patterns of alterations in proton efflux from goldfish retinal horizontal cells monitored with self-referencing H^+-selective electrodes. *Eur J Neurosci* **36,** 3040–3050.

Kurz-Isler G, Voigt T & Wolburg H (1992). Modulation of connexon densities in gap junctions of horizontal cell perikarya and axon terminals in fish retina: effects of light/dark cycles, interruption of the optic nerve and application of dopamine. *Cell Tissue Res* **268,** 267–275.

Kwak S & Weiss JH (2006). Calcium-permeable AMPA channels in neurodegenerative disease and ischemia. *Curr Opin Neurobiol* **16,** 281–287.

Lam DM & Ayoub GS (1983). Biochemical and biophysical studies of isolated horizontal cells from the teleost retina. *Vision Res* **23,** 433–444.

Lasater EM & Dowling JE (1985). Dopamine decreases conductance of the electrical junctions between cultured retinal horizontal cells. *Proc Natl Acad Sci U S A* **82,** 3025–3029.

Lenkowski JR & Raymond P a (2014). Müller glia: Stem cells for generation and regeneration of retinal neurons in teleost fish. *Prog Retin Eye Res* **40,** 94–123.

Linn CL & Gafka a C (2001). Modulation of a voltage-gated calcium channel linked to activation of glutamate receptors and calcium-induced calcium release in the catfish retina. *J Physiol* **535,** 47–63.

Lipton P (1999). Ischemic cell death in brain neurons. *Physiol Rev* **79,** 1431–1568.

Liu X, Hirano A a, Sun X, Brecha NC & Barnes S (2013). Calcium channels in rat horizontal cells regulate feedback inhibition of photoreceptors through an unconventional GABA- and pH-sensitive mechanism. *J Physiol* **591,** 3309–3324.

Lushchak VI, Lushchak LP, Mota AA & Hermes-Lima M (2001). Oxidative stress and antioxidant defenses in goldfish Carassius auratus during anoxia and reoxygenation. *Am J Physiol Regul Integr Comp Physiol* **280,** R100–R107.

Lutz PL & Nilsson GE (1997). Contrasting strategies for anoxic brain survival--glycolysis up or down. *J Exp Biol* **200,** 411–419.

Lutz PL, Nilsson GE & Peréz-Pinzón M a. (1996). Anoxia tolerant animals from a neurobiological perspective. *Comp Biochem Physiol Part B Biochem Mol Biol* **113,** 3–13.

Lv T, Gong H-Q & Liang P-J (2014). Caffeine-induced Ca^{2+} oscillations in type I horizontal cells of the carp retina and the contribution of the store-operated Ca^{2+} entry pathway. *PLoS One* **9,** e100095.

MacVicar BA & Thompson RJ (2010). Non-junction functions of pannexin-1 channels. *Trends Neurosci* **33,** 93–102.

Mandic M, Lau GY, Nijjar MMS & Richards JG (2008). Metabolic recovery in goldfish: A comparison of recovery from severe hypoxia exposure and exhaustive exercise. *Comp Biochem Physiol C Toxicol Pharmacol* **148,** 332–338.

Marc RE (1982). Spatial organization of neurochemically classified interneurons of the goldfish retina-I. Local patterns. *Vision Res* **22,** 589–608.

Marshak DW & Dowling JE (1987). Synapses of cone horizontal cell axons in goldfish retina. *J Comp Neurol* **256,** 430–443.

McMahon DG & Mattson MP (1996). Horizontal cell electrical coupling in the giant danio: synaptic modulation by dopamine and synaptic maintenance by calcium. *Brain Res* **718,** 89–96.

Murakami M & Takahashi K (1987). Calcium action potential and its use for measurement of reversal potentials of horizontal cell responses in carp retina. *J Physiol* **386,** 165–180.

Murakami M & Takahashi K-I (1988). Calcium action potentials in retinal cells of the carp. *Neurosci Res Suppl* **8,** S137–S149.

Nikinmaa M (2002). Oxygen-dependent cellular functions--why fishes and their aquatic environment are a prime choice of study. *Comp Biochem Physiol A Mol Integr Physiol* **133,** 1–16.

Nilsson G & Lutz P (2004). Anoxia tolerant brains. *J Cereb Blood Flow Metab*475–486.

Nilsson GE (2001). Surviving anoxia with the brain turned on. *News Physiol Sci* **16,** 217–221.

Nilsson GE & Lutz PL (1993). Role of GABA in hypoxia tolerance, metabolic depression and hibernation--possible links to neurotransmitter evolution. *Comp Biochem Physiol C* **105,** 329–336.

Nilsson GE, Pérez-Pinzón M, Dimberg K & Winberg S (1993). Brain sensitivity to anoxia in fish as reflected by changes in extracellular K^+ activity. *Am J Physiol* **264,** R250–R253.

Norris CM, Blalock EM, Thibault O, Brewer LD, Clodfelter G V, Porter NM & Landfield PW (2006). Electrophysiological mechanisms of delayed excitotoxicity: positive feedback loop between NMDA receptor current and depolarization-mediated glutamate release. *J Neurophysiol* **96,** 2488–2500.

Ogilvie DM (1982). Behavioral response of goldfish (*Carassius auratus*) to deoxygenated water. *Copeia* **1982,** 434.

Okada T, Schultz K, Geurtz W, Hatt H & Weiler R (1999). AMPA-preferring receptors with high Ca^{2+} permeability mediate dendritic plasticity of retinal horizontal cells. *Eur J Neurosci* **11,** 1085–1095.

Osborne NN, Casson RJ, Wood JPM, Chidlow G, Graham M & Melena J (2004). Retinal ischemia: mechanisms of damage and potential therapeutic strategies. *Prog Retin Eye Res* **23,** 91–147.

Padilla P a & Roth MB (2001). Oxygen deprivation causes suspended animation in the zebrafish embryo. *Proc Natl Acad Sci U S A* **98,** 7331–7335.

Paik S-S, Park N-G, Lee S-J, Han H-K, Jung C-S, Bai S-H & Chun M-H (2003). GABA receptors on horizontal cells in the goldfish retina. *Vision Res* **43,** 2101–2106.

Pamenter ME (2014). Mitochondria: a multimodal hub of hypoxia tolerance 1. *Can J Zool* **92,** 569–589.

Pamenter ME, Hogg DW, Gu XQ, Buck LT & Haddad GG (2012). Painted turtle cortex is resistant to an in vitro mimic of the ischemic mammalian penumbra. *J Cereb Blood Flow Metab* **32,** 2033–2043.

Pamenter ME, Shin DS-H & Buck LT (2008*a*). AMPA receptors undergo channel arrest in the anoxic turtle cortex. *Am J Physiol Regul Integr Comp Physiol* **294,** R606–R613.

Pamenter ME, Shin DS-H, Cooray M & Buck LT (2008*b*). Mitochondrial ATP-sensitive K^+ channels regulate NMDAR activity in the cortex of the anoxic western painted turtle. *J Physiol* **586,** 1043–1058.

Parthe V (1972). Horizontal, bipolar and oligopolar cells in the teleost retina. *Vision Res* **12,** 395–406.

Peng YW, Blackstone CD, Huganir RL & Yau KW (1995). Distribution of glutamate receptor subtypes in the vertebrate retina. *Neuroscience* **66,** 483–497.

Pérez-Pinzón M a, Rosenthal M, Sick TJ, Lutz PL, Pablo J & Mash D (1992). Downregulation of sodium channels during anoxia: a putative survival strategy of turtle brain. *Am J Physiol* **262,** R712–R715.

Piccolino M (1986). Horizontal cells: Historical controversies and new interest. *Prog Retin Res* **5,** 147–163.

Prochnow N, Hoffmann S, Vroman R, Klooster J, Bunse S, Kamermans M, Dermietzel R & Zoidl G (2009). Pannexin1 in the outer retina of the zebrafish, Danio rerio. *Neuroscience* **162,** 1039–1054.

Raynauld JP, Laviolette JR & Wagner HJ (1979). Goldfish retina: a correlate between cone activity and morphology of the horizontal cell in clone pedicules. *Science* **204,** 1436–1438.

Renshaw GMC & Nikinmaa M (2007). 11 Oxygen sensors of the peripheral and central nervous systems.

Robinson E, Jerrett A, Black S & Davison W (2013). Hypoxia impairs visual acuity in snapper (Pagrus auratus). *J Comp Physiol A Neuroethol Sens Neural Behav Physiol* **199,** 611–617.

Rowe JS (1987). Effects of external calcium on horizontal cells in the superfused goldfish retina. *Neurosci Res Suppl* **6,** S147–S163.

Scemes E, Spray DC & Meda P (2009). Connexins, pannexins, innexins: novel roles of "hemi-channels". *Pflugers Arch* **457,** 1207–1226.

Schmidt K-G, Bergert H & Funk RHW (2008). Neurodegenerative diseases of the retina and potential for protection and recovery. *Curr Neuropharmacol* **6,** 164–178.

Schmitz Y, Kohler K & Zrenner E (1995). Evidence for calcium/calmodulin dependence of spinule retraction in retinal horizontal cells. *Vis Neurosci* **12,** 413–424.

Shin DS-H, Wilkie MP, Pamenter ME & Buck LT (2005). Calcium and protein phosphatase 1/2A attenuate N-methyl-D-aspartate receptor activity in the anoxic turtle cortex. *Comp Biochem Physiol A Mol Integr Physiol* **142,** 50–57.

Shingai R & Christensen BN (1986). Excitable properties and voltage-sensitive ion conductances of horizontal cells isolated from catfish (*Ictalurus punctatus*) retina. *J Neurophysiol* **56,** 32–49.

Shoubridge E & Hochachka P (1980). Ethanol: novel end product of vertebrate anaerobic metabolism. *Science* **209,** 308–309.

Solessio E & Lasater EM (2002). Calcium-induced calcium release and calcium buffering in retinal horizontal cells. *Vis Neurosci* **19,** 713–725.

Staples JF & Buck LT (2009). Matching cellular metabolic supply and demand in energy-stressed animals. *Comp Biochem Physiol A Mol Integr Physiol* **153,** 95–105.

Stell WK (1967). The structure and relationships of horizontal cells and photoreceptor-bipolar synaptic complexes in goldfish retina. *Am J Anat* **121,** 401–423.

Stell WK (1975). Horizontal cell axons and axon terminals in goldfish retina. *J Comp Neurol* **159,** 503–520.

Stell WK & Lightfoot DO (1975). Color-specific interconnections of cones and horizontal cells in the retina of the goldfish. *J Comp Neurol* **159,** 473–502.

Stensløkken K, Milton SL, Lutz PL, Sundin L, Renshaw GMC, Stecyk JAW & Nilsson GE (2008*a*). Effect of anoxia on the electroretinogram of three anoxia-tolerant vertebrates. *Comp Biochem Physiol A Mol Integr Physiol* **150,** 395–403.

Stensløkken K-O, Ellefsen S, Stecyk JW, Dahl MB, Nilsson GE & Vaage J (2008*b*). Differential regulation of AMP-activated kinase and AKT kinase in response to oxygen availability in crucian carp (*Carassius carassius*). *Am J Physiol Regul Integr Comp Physiol* **295,** R1803–R1814.

Stensløkken K-O, Ellefsen S, Vasieva O, Fang Y, Farrell AP, Olohan L, Vaage J, Nilsson GE & Cossins AR (2014). Life without oxygen: gene regulatory responses of the crucian carp (*Carassius carassius*) heart subjected to chronic anoxia. *PLoS One* **9,** e109978.

Sun Y, Jiang X-D, Liu X, Gong H-Q & Liang P-J (2010). Synaptic contribution of Ca^{2+}-permeable and Ca^{2+}-impermeable AMPA receptors on isolated carp retinal horizontal cells and their modulation by Zn2+. *Brain Res* **1317,** 60–68.

Svaetichin G & MacNichol EF (1959). Retinal mechanisms for chromatic and achromatic vision. *Ann N Y Acad Sci* **74,** 385–404.

Szabadfi K, Mester L, Reglodi D, Kiss P, Babai N, Racz B, Kovacs K, Szabo A, Tamas A, Gabriel R & Atlasz T (2010). Novel neuroprotective strategies in ischemic retinal lesions. *Int J Mol Sci* **11,** 544–561.

Tachibana M (1981). Membrane properties of solitary horizontal cells isolated from goldfish retina. *J Physiol* **321,** 141–161.

Tachibana M (1983). Ionic currents of solitary horizontal cells isolated from goldfish retina. *J Physiol* **345,** 329–351.

Tachibana M (1985). Permeability changes induced by L-glutamate in solitary retinal horizontal cells isolated from *Carassius auratus*. *J Physiol* **358,** 153–167.

Takahashi K, Dixon DB & Copenhagen DR (1993). Modulation of a sustained calcium current by intracellular pH in horizontal cells of fish retina. *J Gen Physiol* **101,** 695–714.

Tao L & Harris AL (2007). 2-Aminoethoxydiphenylborate directly inhibits channels composed of connexin26 and/or connexin32. *Mol Pharmacol* **71,** 570–579.

Teranishi T, Negishi K & Kato S (1983). Dopamine modulates S-potential amplitude and dye-coupling between external horizontal cells in carp retina. *Nature* **301,** 243–246.

Thompson RJ, Zhou N & MacVicar B a (2006). Ischemia opens neuronal gap junction hemichannels. *Science* **312,** 924–927.

Thoreson WB & Mangel SC (2012). Lateral interactions in the outer retina. *Prog Retin Eye Res* **31,** 407–441.

Twig G, Levy H & Perlman I (2003). Color opponency in horizontal cells of the vertebrate retina. *Prog Retin Eye Res* **22,** 31–68.

Tzaneva V, Vadeboncoeur C, Ting J & Perry SF (2014). Effects of hypoxia-induced gill remodelling on the innervation and distribution of ionocytes in the gill of goldfish, Carassius auratus. *J Comp Neurol* **522,** 118–130.

Vandenbranden C & Verweij J (1996). Clearance of neurotransmitter from the cone synaptic cleft in goldfish retina. *Vision Res* **36,** 3859–3874.

Verweij J, Kamermans M, Negishi K & Spekreijse H (1998). GABA sensitivity of spectrally classified horizontal cells in goldfish retina. *Vis Neurosci* **15,** 77–86.

Vessey JP, Stratis AK, Daniels BA, Da Silva N, Jonz MG, Lalonde MR, Baldridge WH & Barnes S (2005). Proton-mediated feedback inhibition of presynaptic calcium channels at the cone photoreceptor synapse. *J Neurosci* **25,** 4108–4117.

Villani L, Carraro S & Guarnieri T (1995). 6,7-Dinitroquinoxaline-2,3-dione but not MK-801 exerts a protective effect against kainic acid neurotoxicity in the goldfish retina. *Neurosci Lett* **192,** 127–131.

Walker RM & Johansen PH (1977). Anaerobic metabolism in goldfish (*Carassius auratus*). *Can J Zool* **55,** 1304–1311.

Walsh PJ, Veauvy CM, McDonald MD, Pamenter ME, Buck LT & Wilkie MP (2007). Piscine insights into comparisons of anoxia tolerance, ammonia toxicity, stroke and hepatic encephalopathy. *Comp Biochem Physiol A Mol Integr Physiol* **147,** 332–343.

Waser W & Heisler N (2005). Oxygen delivery to the fish eye: root effect as crucial factor for elevated retinal PO_2. *J Exp Biol* **208,** 4035–4047.

Weiler R & Zettler F (1979). The axon-bearing horizontal cells in the teleost retina are functional as well as structural units. *Vision Res* **19,** 1261–1268.

Weilinger NL, Tang PL & Thompson RJ (2012). Anoxia-induced NMDA receptor activation opens pannexin channels via Src family kinases. *J Neurosci* **32,** 12579–12588.

Wilkie MP, Pamenter ME, Alkabie S, Carapic D, Shin DSH & Buck LT (2008). Evidence of anoxia-induced channel arrest in the brain of the goldfish (*Carassius auratus*). *Comp Biochem Physiol C Toxicol Pharmacol* **148,** 355–362.

Willmore WG & Storey KB (1997). Antioxidant systems and anoxia tolerance in a freshwater turtle Trachemys scripta elegans. *Mol Cell Biochem* **170**, 177-185.

Yagi T & Kaneko a (1988). The axon terminal of goldfish retinal horizontal cells: a low membrane conductance measured in solitary preparations and its implication to the signal conduction from the soma. *J Neurophysiol* **59,** 482–494.

Zhou ZY, Sugawara K, Hashi R, Muramoto K, Mawatari K, Matsukawa T, Liu ZW, Devadas M & Kato S (2001). Reactive oxygen species uncouple external horizontal cells in the carp retina and glutathione couples them again. *Neuroscience* **102,** 959–967.

Zivkovic G & Buck LT (2010). Regulation of AMPA receptor currents by mitochondrial ATP-sensitive K^+ channels in anoxic turtle neurons. *J Neurophysiol* **104,** 1913–1922.

Zucker CL & Dowling JE (1987). Centrifugal fibres synapse on dopaminergic interplexiform cells in the teleost retina. *Nature* **330,** 166–168.

Appendix

Supplementary Table I: Summary statistics of the distribution of spontaneous calcium transients from isolated horizontal cells. n=279 events over n=5 cells for all metrics (correspond to panels A-E in Fig. 2).

Metric:	Measure:	n=	Min	Max	Mode	Mean:	Standard deviation	Lower 95% CI	Upper 95% CI
Duration:	s	279	8	750	14	25.79	49.35	19.9756	31.6086
Time To Peak:	s	279	2	40	6	7.96	4.58	7.4246	8.5037
Amplitude:	A.U.	279	0.16	1	NA	0.65	0.20	0.6239	0.6707
Flux:	$\int(A.U.)\,dt$	279	0.03	1	NA	0.25	0.18	0.2291	0.2719
Frequency:	Events/5min	40	1	13	NA	6.47	3.51	5.35304	7.59696

Supplementary Table II: Inter-cell variation in spontaneous event parameters. n=279 events over n=5 cells (correspond to panels A-E in Fig. 2). Significantly different parameter values between cells indicated with a "yes" (Kruskal-Wallis test, $p< 0.05$ with Dunn's Multiple Comparisons test on all groups).

	Duration	Time to Peak	Amplitude	Flux	Frequency/5min
			Mean (SD)		
Cell 1	21.25 (16.99)	7.10 (2.54)	0.63 (0.15)	0.18 (0.18)	7.37 (3.20)
Cell 2	18.80 (8.98)	6.28 (2.31)	0.53 (0.20)	0.24 (0.16)	8.50 (2.41)
Cell 3	21.31 (7.28)	7.12 (2.87)	0.69 (1.90)	0.33 (0.14)	8.10 (2.13)
Cell 4	34.19 (23.83)	14.64 (7.79)	0.82 (0.08)	0.21 (0.18)	3.67 (3.61)
Cell 5	128.6(239.25)	14.8 (5.09)	0.90 (0.10)	0.23 (0.36)	2.00 (1.26)

			Multiple Comparisons*:		
P value	< 0.0001	< 0.0001	< 0.0001	< 0.0001	0.0016
Kruskal-Wallis Statistic	55.68	83.42	79.74	80.71	17.45
1 vs. 3	Yes	No	No	Yes	No
1 vs. 4	Yes	Yes	Yes	No	No
1 vs. 5	Yes	Yes	Yes	No	No
2 vs. 3	Yes	No	Yes	Yes	No
2 vs. 4	Yes	Yes	Yes	No	No
2 vs. 5	Yes	Yes	Yes	No	Yes
3 vs. 4	Yes	Yes	Yes	Yes	No
3 vs. 5	No	Yes	Yes	Yes	Yes
4 vs. 5	No	No	No	No	No

* Each comparison made between different cells (cell 1, 2, 3, 4, and 5).

Supplementary Table III: Statistical summary of effects of OGD treatment on spontaneous events. Means presented for Control, OGD, and Post-application groups from Figure 5. P values for Friedman's tests are presented, n=10 cells.

Metric:		Time Period (min)		
		Control	OGD	Post-application
	P value	Mean (SD):	Mean (SD)	Mean (SD)
Duration	0.1873	30.6 (12.35)	23.6 (6.24)	23 (7.10)
TTP	0.1873	13.1 (7.50)	8.9 (3.18)	8.3 (3.97)
Amplitude	<0.0001	0.98 (0.03)	0.50 (0.26)	0.47 (0.23)
Flux	0.0002	0.88 (0.14)	0.40 (0.29)	0.32 (0.26)
Frequency	1.000	4 (3.13)	3.8 (2.66)	3.9 (2.96)
Baseline	0.1066	0.83 (0.12)	0.89 (0.09)	0.81 (0.12)

Supplementary Table IV: Statistical summary of effects of 0 glucose treatment on spontaneous event frequency and calcium baseline concentration. Means presented for Control, 0 glucose, and Post-application groups from Figure 7. P values for Wilcoxon tests are presented, n=6 cells.

Metric:		Time Period (min)	
		Control	OGD
	P-value	Mean (SD):	Mean (SD)
Duration	0.0545	17.17 (7.14)	15.17 (7.44)
TTP	0.1362	8.17 (3.00)	6.00 (2.83)
Amplitude	0.0313	0.94 (0.05)	0.50 (0.19)
Flux	0.0313	0.93 (0.09)	0.45 (0.21)

Supplementary Table V: Statistical summary of effects of 0 treatment on spontaneous event frequency and calcium baseline concentration. Means presented for Control, 0 glucose, and Post-application groups from Figure 7. P values for Friedman's tests are presented, n=8 cells.

Metric:		Time Period (min)		
		Control	OGD	Post-application
	P-value	Mean (SD):	Mean (SD)	Mean (SD)
Frequency	0.0099	5.5 (3.51)	5.37 (3.74)	0.62 (1.77)
Baseline	0.0003	0.39 (0.19)	0.54 (0.17)	0.97 (0.02)

Supplementary Table VI: Statistical summary of effects of Sham treatment on spontaneous events. Means presented for Control, Sham, and Post-application groups from Suppl. Fig. 1. P values for Friedman's tests are presented, n=3 cells.

Metric:		Time Period (min)		
		Control	Sham	Post-application
	P-value	Mean (SD):	Mean (SD)	Mean (SD)
Duration	0.1901	29 (9.64)	18 (6.08)	17.33 (2.52)
TTP	0.1944	10.33 (1.53)	7.33 (3.21)	6.00 (2.65)
Amplitude	0.3611	0.95 (0.03)	0.83 (0.14)	0.84 (0.07)
Flux	0.1944	0.93 (0.03)	0.44 (0.23)	0.44 (0.12)
Frequency	0.0278[1]	5.67 (0.58)	9 (1)	7 (1)
Baseline	0.0278	0.95 (0.03)	0.78 (0.02)	0.71 (0.01)

[1] Dunn's Post-hoc test finds no significant difference between groups.

Supplementary Table VII: Statistical summary of effects of Sham treatment on spontaneous events. Means presented for Control and Sham from Suppl. Fig. 1. P values for Wilcoxon tests are presented, n=4 cells.

Metric:		Time Period (min)	
	P-value	Control Mean (SD):	Sham Mean (SD)
Duration	0.2500	32.25 (10.21)	18.75 (5.19)
TTP	0.0975	13.25 (5.97)	8.0 (2.94)
Amplitude	0.2500	0.96 (0.03)	0.86 (0.12)
Flux	0.1250	0.94 (0.04)	0.44 (0.19)
Frequency	0.125	4.5 (2.38)	9.5 (1.29)
Baseline	0.2500	0.91 (0.08)	0.82 (0.02)

Supplementary Table VIII: Statistical summary of effects of sham treatment on glutamate events over time. Means presented for Control and Sham groups from Figure 8. P values for Wilcoxon tests are presented, n=3 cells.

Metric:		Time Period (min)	
	P-value	Control Mean (SD):	Sham Mean (SD)
Peak Amplitude	0.75	0.85 (0.25)	0.82 (0.28)
Steady-state amplitude	1.0	0.49 (0.17)	0.52 (0.09)

Supplementary Table IX: Statistical summary of effects of 20 min OGD treatment on glutamate events over time. Means presented for Control, Sham, and Post-application groups from Figure 8. P values for Friedman's tests are presented, n=6 cells.

Metric:		Time Period (min)		
	P-value	Control Mean (SD):	Sham Mean (SD)	Post-application Mean (SD)
Peak Amplitude	0.0055	1 (0)	0.60 (0.22)	0.60 (0.36)
Steady-state amplitude	0.1416	0.44 (0.17)	0.38 (0.14)	0.36 (0.16)

Supplementary Figure 1. Time dependence of spontaneous event parameters (sham). Values taken from 5 min before the onset of OGD (Control, n=4 cells), during the last 5 min of the sham treatment (Sham, n=4 cells) and for the 5 min after the cell had time to recover in control solution for 5 min (Post-application, n=3 cells). **(A)** Duration of spontaneous events (s). **(B)** Time of rise from base to peak amplitude (s). **(C)** Amplitude of spontaneous events. **(D)** Area under the curve (AUC, integrated amplitude over time). **(E)** Frequency of event occurrence (counts/5 min period). **(F)** Relative baseline [Ca^{2+}], A significant difference (Friedmans, Dunn's post-hoc test) is marked with an asterisk. No significant difference was found between groups using Friedman's test (panels A-E) using alpha=0.05, n =3 for each group. No significant difference was found between control and sham groups (Panels A-F), Wilcoxon test. Means (red bars). All panels: statistical summary can be found in Suppl. Tables VI and VII.

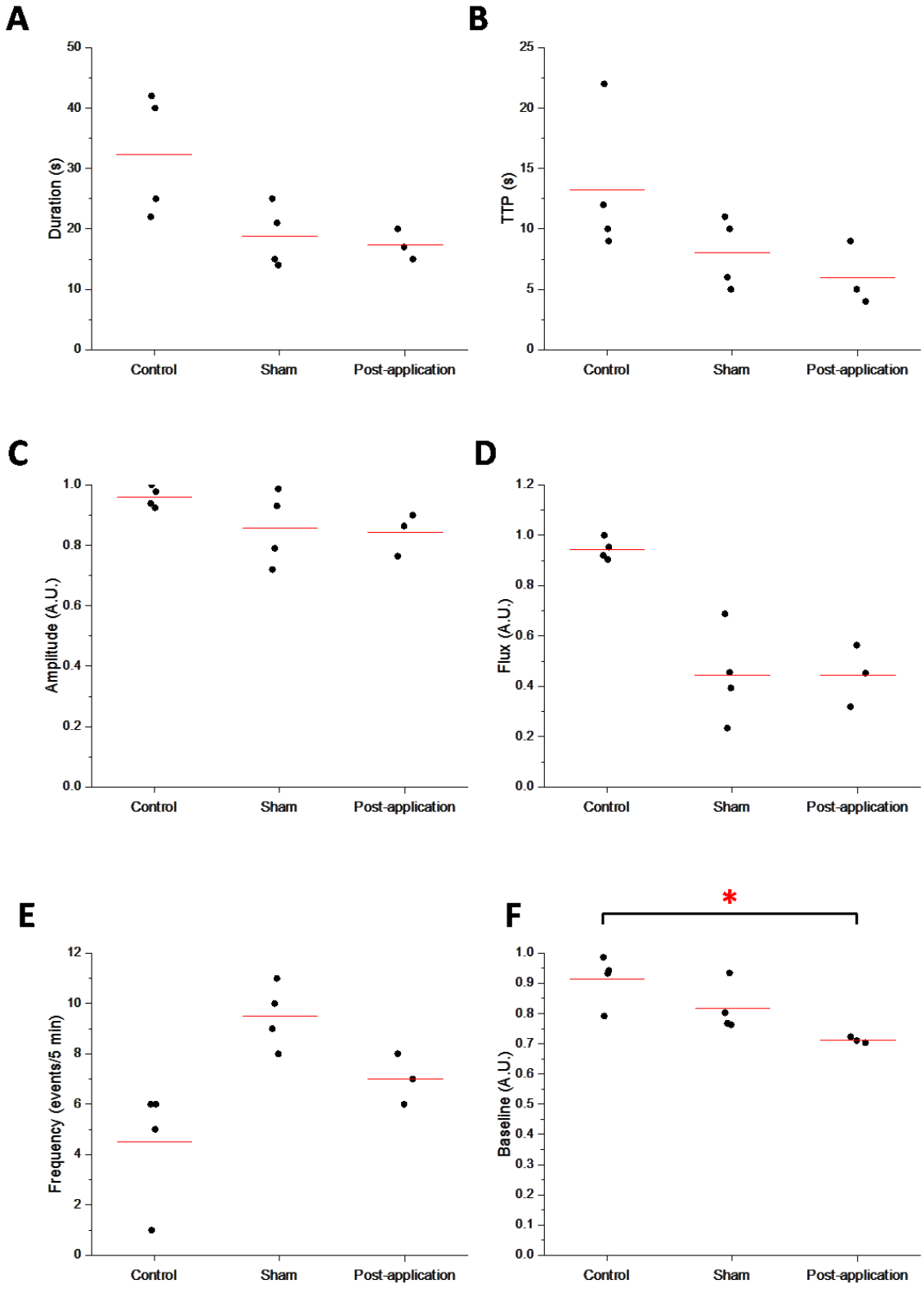
A
Duration (s)
0
10
20
30
40
50
Control
Sham
Post-application
B
TTP (s)
0
5
10
15
20
25
Control
Sham
Post-application
C
Amplitude (A.U.)
0.0
0.2
0.4
0.6
0.8
1.0
Control
Sham
Post-application
D
Flux (A.U.)
0.0
0.2
0.4
0.6
0.8
1.0
1.2
Control
Sham
Post-application
E
Frequency (events/5 min)
0
2
4
6
8
10
12
Control
Sham
Post-application
F
*
Baseline (A.U.)
0.0
0.1
0.2
0.3
0.4
0.5
0.6
0.7
0.8
0.9
1.0
Control
Sham
Post-application

Supplementary Figure 2. Time dependence of glutamate-elicited event parameters (sham). **(A)** Comparison of peak glutamate (100 μM) response amplitude before and after 20 min of normal ECS perfusion, Wilcoxon $p>0.05$, $n=3$ cells. **(B)** Comparison of steady state glutamate response amplitude before and after 20 min of normal ECS perfusion, Wilcoxon, $p>0.05$, $n=3$ cells. Note that glutamate-induced events did not change over a 20 min period. All panels: statistical summary can be found in Suppl. Tables VIII.

A

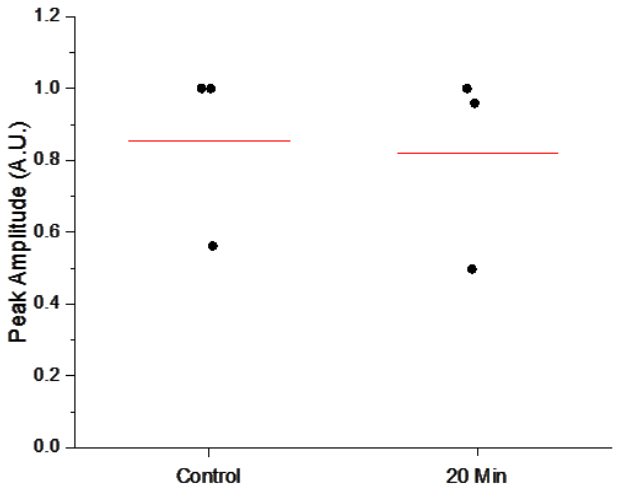
Peak Amplitude (A.U.)
1.2
1.0
0.8
0.6
0.4
0.2
0.0
Control
20 Min

B

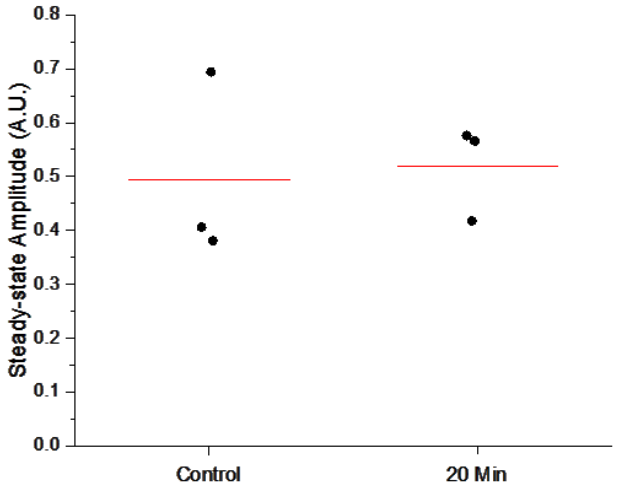
Steady-state Amplitude (A.U.)
0.8
0.7
0.6
0.5
0.4
0.3
0.2
0.1
0.0
Control
20 Min